

Importance sampling for a robust and efficient multilevel Monte Carlo estimator for stochastic reaction networks

Chiheb Ben Hammouda* Nadhir Ben Rached[†] Raúl Tempone^{‡§}

Abstract

The multilevel Monte Carlo (MLMC) method for continuous-time Markov chains, first introduced by Anderson and Higham [3], is a highly efficient simulation technique that can be used to estimate various statistical quantities for stochastic reaction networks (SRNs), in particular for stochastic biological systems. Unfortunately, the robustness and performance of the multilevel method can be affected by the high kurtosis, a phenomenon observed at the deep levels of MLMC, which leads to inaccurate estimates of the sample variance. In this work, we address cases where the high-kurtosis phenomenon is due to *catastrophic coupling* (characteristic of pure jump processes where coupled consecutive paths are identical in most of the simulations, while differences only appear in a tiny proportion) and introduce a pathwise-dependent importance sampling (IS) technique that improves the robustness and efficiency of the multilevel method. Our theoretical results, along with the conducted numerical experiments, demonstrate that our proposed method significantly reduces the kurtosis of the deep levels of MLMC, and also improves the strong convergence rate from $\beta = 1$ for the standard case (without IS), to $\beta = 1 + \delta$, where $0 < \delta < 1$ is a user-selected parameter in our IS algorithm. Due to the complexity theorem of MLMC, and given a pre-selected tolerance, TOL, this results in an improvement of the complexity from $\mathcal{O}(\text{TOL}^{-2} \log(\text{TOL})^2)$ in the standard case to $\mathcal{O}(\text{TOL}^{-2})$, which is the optimal complexity of the MLMC estimator. We achieve all these improvements with a negligible additional cost since our IS algorithm is only applied a few times across each simulated path.

Keywords Multilevel Monte Carlo. Continuous-time Markov chains. Stochastic reaction networks. Stochastic biological systems. Importance sampling.

2010 Mathematics Subject Classification 60H35. 60J27. 60J75. 92C40.

1 Introduction

In this work, we propose a novel importance sampling (IS) algorithm that can be combined with the multilevel Monte Carlo (MLMC) estimator to numerically solve stochastic differential equations (SDEs) driven by Poisson random measures [34, 14].

*King Abdullah University of Science and Technology (KAUST), Computer, Electrical and Mathematical Sciences & Engineering Division (CEMSE), Thuwal 23955 – 6900, Saudi Arabia (chiheb.benhammouda@kaust.edu.sa).

[†]Chair of Mathematics for Uncertainty Quantification, RWTH Aachen University, Aachen 52072, Germany. (benrached@uq.rwth-aachen.de).

[‡]King Abdullah University of Science and Technology (KAUST), Computer, Electrical and Mathematical Sciences & Engineering Division (CEMSE), Thuwal 23955 – 6900, Saudi Arabia (raul.tempone@kaust.edu.sa).

[§]Alexander von Humboldt Professor in Mathematics for Uncertainty Quantification, RWTH Aachen University, Aachen 52072, Germany.

We focus on a particular class of continuous-time Markov chains known as stochastic reaction networks (SRNs) (see Section 1.1 for a short introduction). SRNs describe the time evolution of biochemical reactions, epidemic processes [11, 7], and transcription and translation in genomics and virus kinetics [40, 28], among other important applications.

Let \mathbf{X} be an SRN taking values in \mathbb{N}^d and defined in the time-interval $[0, T]$, where $T > 0$ is a user-selected final time. We aim to provide accurate MLMC estimations of the expected value, $E[g(\mathbf{X}(T))]$, where $g : \mathbb{R}^d \rightarrow \mathbb{R}$ is a given scalar observable of \mathbf{X} .

The main goal of our new proposed method is to improve the robustness and performance of the MLMC estimator by i) solving the high-kurtosis phenomenon encountered when using the multilevel method in the context of continuous-time Markov chains (see Section 1.4), and ii) improving the complexity of the MLMC estimator by increasing the strong convergence rate.

Many methods have been developed to simulate exact sample paths of SRNs; for instance, the stochastic simulation algorithm (SSA) was introduced by Gillespie in [22] and the modified next reaction method (MNRM) was proposed by Anderson in [4]. Pathwise exact realizations of SRNs may be computationally very costly when some reaction channels have high reaction rates. To overcome this issue, Gillespie [24] and Aparicio and Solari [8] independently proposed the explicit tau-leap (TL) method (see Section 1.2) to simulate approximate paths of \mathbf{X} by evolving the process with fixed time steps, keeping the reaction rates fixed within each time step. Furthermore, other simulation schemes have been proposed to deal with situations with well-separated fast and slow time scales [12, 39, 1, 2, 35, 27].

To reduce the computational work needed to estimate $E[g(\mathbf{X}(T))]$, Anderson and Higham [3] introduced the MLMC method [20, 21] based on the explicit TL scheme in the context of SRNs. Many extensions of the MLMC method have since been introduced to address other challenges. For instance, adaptive multilevel estimators [33, 36, 35] were proposed to improve the performance of non-adaptive estimators [3] to simulate SRNs with markedly different time scales. [27] extended [3] to systems with slow and fast time scales, and introduced a hybrid multilevel estimator that uses an implicit scheme for levels where explicit TL cannot be used due to numerical instability.

One important challenge encountered when using MLMC in the context of SRNs is the high-kurtosis phenomenon (see Section 1.4 for more details), which may occur due to either *catastrophic coupling* (characteristic of pure jump processes where coupled consecutive paths are identical in most of the simulations, while differences only appear in a tiny proportion; see Section 1.4.1 for more details) or *catastrophic decoupling* (observed for general stochastic processes where terminal values of the sample paths of both coarse and fine levels become very different from each other; see Section 1.4.2 for more details). This poor behavior of the kurtosis affects the accurate estimation of the sample variance needed for the MLMC algorithm. Consequently, it affects the robustness and performance of the multilevel estimator in many cases (see Section 1.4 for the illustration of this issue). As of today, few works have addressed this issue; for instance, the authors in [36] mentioned this issue and developed a more accurate estimator for the multilevel variance based on dual-weighted residual expansion techniques. In [32], a new method has been proposed to address the high-kurtosis phenomenon when it is due to *catastrophic decoupling*, and introduced a new approach of coupling consecutive levels of MLMC called the *common process method* (CPM), instead of using the *split propensity method* (SPM) proposed in [3]. The CPM is based on the use of common inhomogeneous Poisson processes for both coarse and fine sample paths. Although the CPM improves the robustness and reliability of the multilevel estimator by dramatically decreasing the kurtosis, it nonetheless incurs remarkable additional computational and memory costs because

for each level it requires i) running the TL algorithm twice, and ii) storing the total number of times each Poisson process has fired over each time step.

In the work presented here, compared to [32], we address cases of high kurtosis observed in the MLMC estimator due to *catastrophic coupling* and propose a novel method that provides a more robust multilevel estimator. We introduce a pathwise-dependent IS technique to dramatically decrease the high kurtosis caused by the SPM strategy for coupling the paths of two consecutive levels. We should note that other IS methods were proposed, in the context of biochemical systems and SRNs, but for the efficient estimation of rare events [30, 16, 13]. Furthermore, these IS methods were combined with the MC method instead of the MLMC method that we present here.

We show that our proposed method not only improves the robustness of the multilevel estimator by significantly reducing the kurtosis, but also improves the strong convergence rate from $\beta = 1$ for the standard case (without IS), to $\beta = 1 + \delta$, where $0 < \delta < 1$ is a user-selected parameter in our IS algorithm. Due to the complexity theorem of MLMC [15], and given a pre-selected tolerance, TOL, this results in an improvement of the complexity of MLMC from $\mathcal{O}(\text{TOL}^{-2} \log(\text{TOL})^2)$ to the optimal complexity, *i.e.*, $\mathcal{O}(\text{TOL}^{-2})$. We achieve all these improvements with a negligible additional cost since our IS algorithm is only applied a few times across each simulated path.

Alternatively, the optimal MLMC complexity of order $\mathcal{O}(\text{TOL}^{-2})$ can be achieved by using (i) MC with an exact scheme (for instance SSA), or (ii) an unbiased MLMC estimator [3], where the deepest level is simulated with an exact scheme, or (iii) a biased hybrid MLMC estimator [36], where the paths are simulated in a hybrid fashion that switches adaptively, based on the relative computational cost, between the TL and an exact method. Both approaches (i) and (ii) incur a substantial additional cost by introducing an exact scheme. This significant additional cost is not manifested in the rate exponent but in a large constant that deteriorates the actual complexity. Although our method is based on a biased MLMC estimator, without steps simulated with an exact scheme as in [36], it still achieves a complexity of order $\mathcal{O}(\text{TOL}^{-2})$ with a smaller constant than those produced by the methods (i), (ii) and (iii) mentioned above. Compared to [3], we suggest an orthogonal approach of lowering the complexity rate by improving the strong convergence rate, instead of removing the bias (weak error). Similarly to our work, the authors in [36] improve the strong convergence rate to reach the complexity of order $\mathcal{O}(\text{TOL}^{-2})$. However, compared to [36], we use a different strategy based on a pathwise-dependent IS coupled with the TL scheme, instead of using a hybrid approach that switches between an exact and the TL scheme.

We also propose a new approach to overcome the high-kurtosis phenomenon, which affects the robustness and reliability of the MLMC estimator introduced in [3]. Although this issue can be addressed differently, using the dual-weighted residual expansion techniques developed in [36] in order to estimate more accurately the sample variance and bias on the deepest levels of MLMC, we believe that our approach has two main advantages over the approach in [36]: first, our method is much simpler and easier to generalize to other schemes, such as the split-step implicit TL scheme [27] where it is difficult to get estimates using the dual-weighted residual expansion techniques. Furthermore, although the approach in [36] provides a more accurate estimate of the variance than the sample variance estimate, there is still no clear analysis of how accurate (biased) those estimates are. The difficulty of establishing such analysis is mainly due to the lack of sharp concentration inequalities for linear combinations of independent Poisson random variables (rdvs), as stated in Remark 4 in [36]. Finally, we should emphasize that the hybrid scheme in [36] is an efficient algorithm that avoids the simulated paths to take negative values, which is an undesirable consequence of the TL approximation. In this case, for problems where we are close to the boundary, combining

the two approaches (our approach and the approach in [36]) may lead to more efficient results.

This work is structured as follows: we start by giving an overview of concepts used in this work such as SRNs (Section 1.1), explicit TL approximation (Section 1.2), and the MLMC method (Section 1.3). Then, in Section 1.4, we explain the high-kurtosis phenomenon along with its leading causes in the context of SRNs. In Sections 2, 3 and, 4, we present the details of our IS algorithm that we combine with the MLMC method. We start by presenting in Section 2 the motivation of our idea by the sampling under an optimal measure for simulating SRNs. Then, in Section 3, we present a summary of the main results of this work, and in Section 4, we analyze our proposed IS algorithm and state the main convergence theorems related to the kurtosis and the variance estimates of our approach. Furthermore, we present, in the same section, a cost analysis of the MLMC methods presented in this work, with and without IS. Before concluding, we show, in Section 5, the results obtained through the numerical experiments conducted across different examples of SRNs.

1.1 Stochastic Reaction Networks (SRNs)

We are interested in the time evolution of a homogeneously mixed chemical reacting system described by the Markovian pure jump process, $\mathbf{X} : [0, T] \times \Omega \rightarrow \mathbb{N}^d$, where (Ω, \mathcal{F}, P) is a probability space. In this framework, we assume that d different species interact through J reaction channels. The i -th component, $X^{(i)}(t)$, describes the abundance of the i -th species present in the chemical system at time t . This work aims to study the time evolution of the state vector,

$$\mathbf{X}(t) = (X^{(1)}(t), \dots, X^{(d)}(t)) \in \mathbb{N}^d.$$

Each reaction channel, \mathcal{R}_j , is a pair $(a_j, \boldsymbol{\nu}_j)$ defined by its propensity function, $a_j : \mathbb{R}^d \rightarrow \mathbb{R}_+$, and its state change vector, $\boldsymbol{\nu}_j = (\nu_{j,1}, \nu_{j,2}, \dots, \nu_{j,d})$, satisfying¹

$$(1.1) \quad \text{Prob}(\mathbf{X}(t + \Delta t) = \mathbf{x} + \boldsymbol{\nu}_j; \mathbf{X}(t) = \mathbf{x}) = a_j(\mathbf{x})\Delta t + o(\Delta t), \quad j = 1, 2, \dots, J.$$

Formula (1.1) states that the probability of observing a jump in the process, \mathbf{X} , from state \mathbf{x} to state $\mathbf{x} + \boldsymbol{\nu}_j$, a consequence of the firing of reaction \mathcal{R}_j during a small time interval, $(t, t + \Delta t]$, is proportional to the length of the time interval, Δt , with $a_j(\mathbf{x})$ as the constant of proportionality.

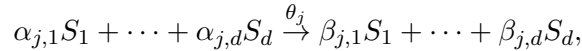
We set $a_j(\mathbf{x})=0$ for \mathbf{x} such that $\mathbf{x} + \boldsymbol{\nu}_j \notin \mathbb{N}^d$ (*the non-negativity assumption*: the system can never produce negative population values).

As a consequence of relation (1.1), the process \mathbf{X} is a continuous-time, discrete-space Markov chain that can be characterized by the random time change representation of Kurtz [19]

$$(1.2) \quad \mathbf{X}(t) = \mathbf{x}_0 + \sum_{j=1}^J Y_j \left(\int_0^t a_j(\mathbf{X}(s)) \, ds \right) \boldsymbol{\nu}_j,$$

where $Y_j : \mathbb{R}_+ \times \Omega \rightarrow \mathbb{N}$ are independent unit-rate Poisson processes. Conditions on the reaction channels can be imposed to ensure uniqueness [7] and to avoid explosions in finite time [18, 38, 26].

We emphasize that, by using the *stochastic mass-action kinetics* principle, we assume that the propensity function, $a_j(\cdot)$, for a reaction channel \mathcal{R}_j , represented by the following diagram²



¹Hereafter, we use $\text{Prob}(A; B)$ and $\mathbb{E}[A; B]$ to denote the conditional probability and conditional expectation of A given B , respectively.

² $\alpha_{j,i}$ molecules of the species S_i are consumed and $\beta_{j,i}$ are produced. Thus, $(\alpha_{j,i}, \beta_{j,i}) \in \mathbb{N}^2$ but $\beta_{j,i} - \alpha_{j,i}$, can be a negative integer, constituting the vector $\boldsymbol{\nu}_j = (\beta_{j,1} - \alpha_{j,1}, \dots, \beta_{j,d} - \alpha_{j,d}) \in \mathbb{Z}^d$.

obeys the following relation

$$(1.3) \quad a_j(\mathbf{x}) := \theta_j \prod_{i=1}^d \frac{x_i!}{(x_i - \alpha_{j,i})!} \mathbf{1}_{\{x_i \geq \alpha_{j,i}\}},$$

where $\{\theta_j\}_{j=1}^J$ are positive constant reaction rates, x_i is the counting number of the species S_i , and $\mathbf{1}_{\mathcal{A}}$ is the indicator function of the set \mathcal{A} .

1.2 The Explicit Tau-Leap (Explicit-TL) Approximation

The explicit-TL scheme is a pathwise-approximate method independently introduced in [24] and [8] to overcome the computational drawback of exact methods, *i.e.*, when many reactions fire during a short time interval. This scheme can be derived from the random time change representation of Kurtz (1.2) by approximating the integral $\int_{t_i}^{t_{i+1}} a_j(\mathbf{X}(s)) ds$ by $a_j(\mathbf{X}(t_i))(t_{i+1} - t_i)$, *i.e.*, using the forward-Euler method with a time mesh $\{t_0 = 0, t_1, \dots, t_N = T\}$. In this way, the explicit-TL approximation of \mathbf{X} should satisfy for $k \in \{1, 2, \dots, N\}$

$$\mathbf{Z}(t_k) = \mathbf{x}_0 + \sum_{j=1}^J Y_j \left(\sum_{i=0}^{k-1} a_j(\mathbf{Z}(t_i))(t_{i+1} - t_i) \right) \boldsymbol{\nu}_j.$$

Given a uniform time mesh of size Δt and $\mathbf{Z}(t_0) := \mathbf{x}_0$, we simulate a path of \mathbf{Z} as follows

$$\mathbf{Z}(t_k) := \mathbf{z} + \sum_{j=1}^J \mathcal{P}_j(a_j(\mathbf{z})\Delta t) \boldsymbol{\nu}_j, \quad 1 \leq k \leq N,$$

iteratively, where $\mathbf{z} = \mathbf{Z}(t_{k-1})$ and $\{\mathcal{P}_j(r_j)\}_{j=1}^J$ are independent Poisson rdvs with respective rates, r_j . Note that the explicit-TL path, \mathbf{Z} , is defined only at the points of the time mesh, but it can be naturally extended to $[0, T]$ as a piecewise constant path.

1.3 The Multilevel Monte Carlo (MLMC) Method

Let \mathbf{X} be a stochastic process and $g : \mathbb{R}^d \rightarrow \mathbb{R}$ a scalar observable. Let us assume that we want to approximate $\mathbb{E}[g(\mathbf{X}(T))]$, but instead of sampling directly from $\mathbf{X}(T)$, we sample from $\mathbf{Z}_{\Delta t}(T)$, which are rdvs generated by an approximate method with step size Δt . Let us also assume that the variates $\mathbf{Z}_{\Delta t}(T)$ are generated with an algorithm with weak order, $\mathcal{O}(\Delta t)$, *i.e.*, $\mathbb{E}[g(\mathbf{X}(T)) - g(\mathbf{Z}_{\Delta t}(T))] = \mathcal{O}(\Delta t)$.³

Let μ_M be the standard Monte Carlo estimator of $\mathbb{E}[g(\mathbf{Z}_{\Delta t}(T))]$ defined by

$$\mu_M := \frac{1}{M} \sum_{m=1}^M g(\mathbf{Z}_{\Delta t, [m]}(T)),$$

where $\{\mathbf{Z}_{\Delta t, [m]}(T)\}_{m=1}^M$ are independent and distributed as $\mathbf{Z}_{\Delta t}(T)$.

³We refer to [34] for the underlying assumptions and proofs of this statement, in the context of the TL scheme.

We define the global error of the MC estimator as $\left(\mathbb{E} \left[(\mathbb{E} [g(\mathbf{X}(T))] - \mu_M)^2 \right] \right)^{\frac{1}{2}}$. Then, we write the following error decomposition

$$\mathbb{E} \left[(\mathbb{E} [g(\mathbf{X}(T))] - \mu_M)^2 \right] = \underbrace{\mathbb{E} [g(\mathbf{X}(T)) - g(\mathbf{Z}_{\Delta t}(T))]^2}_{\text{squared bias}} + \underbrace{\mathbb{E} [g(\mathbf{Z}_{\Delta t}(T)) - \mu_M]^2}_{\text{Variance}}.$$

To achieve the desired accuracy, TOL, it is sufficient to take $\Delta t = \mathcal{O}(\text{TOL})$ so that the bias is $\mathcal{O}(\text{TOL})$ and impose $M = \mathcal{O}(\text{TOL}^{-2})$ so that the variance is $\mathcal{O}(\text{TOL})$ [17]. As a consequence, the expected total computational work is $\mathcal{O}(\text{TOL}^{-3})$.

The MLMC estimator, introduced by Giles [20] (see also [29] for the two-level construction), allows us to reduce the total computational work up to $\mathcal{O} \left(\text{TOL}^{-2-\max(0, \frac{\gamma-\beta}{\alpha}) \log(\text{TOL})^{2 \times \mathbf{1}_{\{\beta=\gamma\}}}} \right)$, where (α, β, γ) are weak, strong, and work rates, respectively (see Theorem 1.1 for more details). The basic idea of MLMC is to generate, and couple in a clever manner, paths with different step sizes. We can construct the MLMC estimator as follows: consider a hierarchy of nested meshes of the time interval $[0, T]$, indexed by $\ell = 0, 1, \dots, L$. We denote by Δt_0 the step size used at level $\ell = 0$. The size of the subsequent time steps for levels $\ell \geq 1$ is given by $\Delta t_\ell = K^{-\ell} \Delta t_0$, where $K > 1$ is a given integer constant. In this work, we take $K = 2$. Furthermore, we denote by M_ℓ the number of samples per level in the MLMC estimator. To simplify the notation, hereafter \mathbf{Z}_ℓ denotes the approximate process generated using a step size of Δt_ℓ .

Consider now the following telescoping decomposition of $\mathbb{E} [g(\mathbf{Z}_L(T))]$

$$(1.4) \quad \begin{aligned} \mathbb{E} [g(\mathbf{Z}_L(T))] &= \mathbb{E} [g(\mathbf{Z}_0(T))] + \sum_{\ell=1}^L \mathbb{E} [g(\mathbf{Z}_\ell(T)) - g(\mathbf{Z}_{\ell-1}(T))] \\ \text{Var}[g(\mathbf{Z}_0(T))] &\gg \text{Var}[g(\mathbf{Z}_\ell(T)) - g(\mathbf{Z}_{\ell-1}(T))] \searrow \text{ as } \ell \nearrow \\ M_0 &\gg M_\ell \searrow \text{ as } \ell \nearrow. \end{aligned}$$

Then, by defining

$$(1.5) \quad \begin{cases} \hat{Q}_0 := \frac{1}{M_0} \sum_{m_0=1}^{M_0} g(\mathbf{Z}_{0,[m_0]}(T)) \\ \hat{Q}_\ell := \frac{1}{M_\ell} \sum_{m_\ell=1}^{M_\ell} (g(\mathbf{Z}_{\ell,[m_\ell]}(T)) - g(\mathbf{Z}_{\ell-1,[m_\ell]}(T))) , \end{cases}$$

we arrive at the unbiased MLMC estimator, \hat{Q} , of $\mathbb{E} [g(\mathbf{Z}_L(T))]$

$$(1.6) \quad \hat{Q} := \sum_{\ell=0}^L \hat{Q}_\ell.$$

We note that the key point here is that both $\mathbf{Z}_{\ell,[m_\ell]}(T)$ and $\mathbf{Z}_{\ell-1,[m_\ell]}(T)$ are sampled using different time discretizations but with the same generated randomness.

Theorem 1.1 from [15] states the computational complexity of the MLMC estimator for different scenarios:

Theorem 1.1 (MLMC complexity). *Let $g := g(\mathbf{X})$ denote a rdv, and let $g_\ell := g(\mathbf{Z}_\ell)$ denote the corresponding level ℓ numerical approximation. If there exist independent estimators \hat{Q}_ℓ based on M_ℓ*

Monte Carlo samples, each with expected cost W_ℓ and variance V_ℓ , and positive constants α (weak convergence rate), β (strong convergence rate), γ (work rate), c_1, c_2, c_3 such that $\alpha \geq \min(\beta, \gamma)$ and

$$i) \quad |\mathbb{E}[g_\ell - g]| \leq c_1 2^{-\alpha\ell}$$

$$ii) \quad \mathbb{E}[\hat{Q}_\ell] = \begin{cases} \mathbb{E}[g_0], & \ell = 0 \\ \mathbb{E}[g_\ell - g_{\ell-1}], & \ell > 0 \end{cases}$$

$$iii) \quad V_\ell := \text{Var}[g_\ell - g_{\ell-1}] \leq c_2 2^{-\beta\ell}$$

$$iv) \quad W_\ell \leq c_3 2^{\gamma\ell},$$

then there exists a positive constant c_4 such that for any $TOL < e^{-1}$, there are values L and M_ℓ for which the multilevel estimator

$$\hat{Q} = \sum_{\ell=0}^L \hat{Q}_\ell,$$

has a mean-square-error with bound

$$\mathbb{E} \left[\left(\hat{Q} - \mathbb{E}[g] \right)^2 \right] < TOL^2,$$

with a computational complexity W with bound

$$\mathbb{E}[W] = \begin{cases} c_4 TOL^{-2}, & \beta > \gamma, \\ c_4 TOL^{-2} (\log(TOL))^2, & \beta = \gamma, \\ c_4 TOL^{-2 - \frac{\gamma - \beta}{\alpha}}, & \beta < \gamma. \end{cases}$$

We emphasize that Theorem 1.1 still applies to our approach, proposed in Section 4, since we only modify the way we sample coupled paths in this context, by combining the standard way of coupling two tau-leap paths with our IS algorithm. Our proposed IS technique does not change the weak rate but improves the strong convergence rate, β , thus leading to an improvement of the MLMC complexity rate, to reach the optimal rate.

1.4 The High-Kurtosis Phenomenon

Let g denote a rdv, and let g_ℓ denote the corresponding level ℓ numerical approximation. We also define $Y_\ell := g_\ell - g_{\ell-1}$. The standard deviation of the sample variance for the rdv Y_ℓ is given by

$$(1.7) \quad \sigma_{S^2(Y_\ell)} = \frac{\sqrt{\text{Var}[Y_\ell]}}{\sqrt{M}} \sqrt{(\kappa - 1) + \frac{2}{M - 1}},$$

where the kurtosis $\kappa = \frac{\mathbb{E}[(Y_\ell - \mathbb{E}[Y_\ell])^4]}{(\text{Var}[Y_\ell])^2}$.

For the setting of the MLMC method, accurate estimates of $V_\ell = \text{Var}[Y_\ell]$ are required since the optimal number of samples per level, M_ℓ^* , for the MLMC estimator is given by (see [21] for more details)

$$(1.8) \quad M_\ell^* = \left\lceil 2TOL^{-2} \sqrt{V_\ell W_\ell^{-1}} \sum_{\ell=L_0}^L \sqrt{V_\ell W_\ell} \right\rceil,$$

where $[x] := \text{ceil}(x)$, W_ℓ is the cost per sample path, TOL is the accuracy of the MLMC estimator, and L_0 ⁴ and L are the coarsest and the deepest levels of the MLMC estimator, respectively.

The high kurtosis makes it challenging to estimate V_ℓ accurately, since $\mathcal{O}(\kappa)$ samples are required to obtain a reasonable estimate of the variance (see 1.7). Two possible consequences of the high kurtosis may occur, and deteriorate the robustness and the performance of the MLMC estimator

- The sample variance, V_ℓ , is an under-estimate. The effect is that the required confidence interval semi-length is not faithfully attained, due to $\sigma_{S^2(Y_\ell)}$ given by (1.7).
- The sample variance, V_ℓ , is an over-estimate. In this case, too many sample paths are generated, and the algorithm takes substantially more time to run.

Several studies [21, 25, 36, 27, 32, 9] discussed the issue of high kurtosis when using MLMC, for different applications. In the context of SRNs, there are mainly two causes of the high-kurtosis phenomenon: i) *Catastrophic coupling* or ii) *Catastrophic decoupling*. In the following subsections, we explain these two causes.

1.4.1 Catastrophic Coupling

The high-kurtosis phenomenon, in this case, is caused by *catastrophic coupling* (see Section 1.7 of [36]), which is a characteristic of pure jump processes that motivates this work. When using the MLMC estimator in this context, the following issue is usually encountered: When ℓ (MLMC level) becomes large, due to the used coupling strategy (see Section 2), Y_ℓ is different from zero only in a tiny proportion of the simulated coupled paths (see Figures 5.3, 5.5 5.7). This behavior is one of the leading causes of the high-kurtosis phenomenon (see Figures 5.2, 5.4 and 5.6), resulting in inaccurate estimates of the sample variance (see (1.7)).

As an illustration of *catastrophic coupling*, consider an example when g takes values in $\{0, 1\}$, and let g_ℓ denote the corresponding level ℓ numerical approximation in the MLMC estimator. In this case, we have

$$(1.9) \quad Y_\ell = g_\ell - g_{\ell-1} = \begin{cases} 1, & \text{with probability } p_\ell \\ -1, & \text{with probability } q_\ell \\ 0, & \text{with probability } 1 - p_\ell - q_\ell. \end{cases}$$

Observe that this example is a true illustration of the SRNs that we consider in this work. For instance, by observing the histograms in Figures 5.3, 5.5 and 5.7, we can check that we usually encounter the situation manifested by (1.9), with $p_\ell, q_\ell \ll 1$, and $\text{Prob}(g_\ell - g_{\ell-1} = 0) \rightarrow 1$ as ℓ increases.

If $p_\ell, q_\ell \ll 1$, then $E[Y_\ell] \approx 0$ and $\kappa_\ell \approx (p_\ell + q_\ell)^{-1} \gg 1$. Therefore, many samples are required for an accurate estimate of $V_\ell = \text{Var}[Y_\ell]$, since using (1.7), we need $M_\ell \gg \kappa_\ell \xrightarrow{\ell \rightarrow \infty} \infty$; otherwise, we may get all samples $Y_\ell = 0$, which gives an estimated variance of zero. Furthermore, the kurtosis becomes worse as $\ell \rightarrow \infty$ since $p_\ell, q_\ell \rightarrow 0$ due to weak convergence.

⁴We set $L_0 = 0$ unless otherwise stated. In our numerical experiments, we select L_0 such that $\text{Var}[g_{L_0+1} - g_{L_0}] \ll \text{Var}[g_{L_0}]$, in order to ensure the stability of the variance of the coupled paths of our MLMC estimator.

1.4.2 Catastrophic Decoupling

The high-kurtosis phenomenon can also occur because of *catastrophic decoupling*, as explained in [31] and observed in [32]. *Catastrophic decoupling* occurs when the terminal values of the sample paths of both coarse and fine levels become very different from each other. In fact, due to the SPM coupling strategy (see Section 2), all reactions start immediately in the fine level and not in the coarse level, since reactions cannot happen until the reaction propensities are updated. We note that this issue becomes more severe when dealing with large scales of species count.

We emphasize that we do not treat *catastrophic decoupling* with our novel proposed method, but rather we address the case of *catastrophic coupling*. Nonetheless, *catastrophic decoupling* can be addressed by using a different coupling, such as CPM coupling [32]. In a future work, to address the issue of *catastrophic decoupling*, we intend to explore the possibility of introducing a new IS scheme for MLMC based on SPM coupling.

Remark 1.1. As proposed in [23], SRNs paths can be approximated using the chemical Langevin equation (CLE), which is only valid when the expected number of occurrences of each reaction channel R_j in $[t, t + \Delta t)$ is much larger than 1, i.e.,

$$(1.10) \quad a_j(\mathbf{x}_t)\Delta t \gg 1, \quad \forall j \in \{0, 1, \dots, J\}.$$

Assumption (1.10), implicitly implies that the system has large molecular population numbers. In this work, we do not impose this restriction on the examples we consider. Moreover, such an assumption does not hold in our setting and more precisely in the deepest level of MLMC estimator (Δt very small).

2 Motivation

2.1 Characterization of the Original Coupling Measure

Let us use the notations of Section 1.3, and denote $g_\ell := g(\mathbf{Z}_\ell(T))$. Then, we can rewrite (1.4) as

$$(2.1) \quad \mathbb{E}[g_L] = \sum_{\ell=1}^L \mathbb{E}[g_\ell - g_{\ell-1}] + \mathbb{E}[g_0],$$

where each term in (2.1) can be written as

$$(2.2) \quad \mathbb{E}[g_0] = \int g_0 d\mathbb{P}_0, \quad \mathbb{E}[g_\ell - g_{\ell-1}] = \int (g_\ell - g_{\ell-1}) d\mathbb{P}_\ell,$$

where \mathbb{P}_ℓ is the coupling measure and \mathbb{P}_0 is the single level measure.

To characterize the original coupling measure \mathbb{P}_ℓ in the context of SRNs, we define the pure jump process X by the Kurtz representation, as in (1.2). For the sake of simplicity, let us consider X to be one-dimensional (only one species), only one reaction ($J = 1$) (in this case we denote the state change scalar by ν_1 ; see (1.1)), and $g(x) = x$, $x \in \mathbb{R}$. We denote $\overline{X}_{\ell-1}, \overline{X}_\ell$ the two TL approximations of the true process X based on two consecutive grid levels $(\ell-1, \ell)$ and recall that $\Delta t_{\ell-1} = 2\Delta t_\ell$ (equivalently, we denote by $N_{\ell-1}$ and N_ℓ the number of time steps used at levels $\ell-1$ and ℓ , respectively). Let $0 \leq n \leq N_{\ell-1} - 1$. If we consider two consecutive time-mesh points

for $\bar{X}_{\ell-1}$, $\{t_n, t_{n+1}\}$, and three consecutive time-mesh points for \bar{X}_ℓ , $\{t_n, t_n + \Delta t_\ell, t_{n+1}\}$, then we have

$$(2.3) \quad \begin{aligned} \bar{X}_{\ell-1}(t_{n+1}) &= \bar{X}_{\ell-1}(t_n) + \nu_1 \mathcal{Y}_{1,n} (a(\bar{X}_{\ell-1}(t_n)) \Delta t_{\ell-1}) \\ \bar{X}_\ell(t_n + \Delta t_\ell) &= \bar{X}_\ell(t_n) + \nu_1 \mathcal{Q}_{1,n} (a(\bar{X}_\ell(t_n)) \Delta t_\ell) \\ \bar{X}_\ell(t_{n+1}) &= \bar{X}_\ell(t_n + \Delta t_\ell) + \nu_1 \mathcal{R}_{1,n} (a(\bar{X}_\ell(t_n + \Delta t_\ell)) \Delta t_\ell), \end{aligned}$$

where $\mathcal{Y}_{1,n}$, $\mathcal{Q}_{1,n}$, $\mathcal{R}_{1,n}$ are conditionally independent Poisson rdvs.

To couple the $\bar{X}_{\ell-1}$ and \bar{X}_ℓ processes, we first decompose $\mathcal{Y}_{1,n} (a(\bar{X}_{\ell-1}(t_n)) \Delta t_{\ell-1})$ as the sum of two conditionally independent Poisson rdvs, $\mathcal{P}_{1,n} (a(\bar{X}_{\ell-1}(t_n)) \Delta t_\ell) + \mathcal{P}_{2,n} (a(\bar{X}_{\ell-1}(t_n)) \Delta t_\ell)$. Then, by applying this decomposition in (2.3), we obtain

$$\begin{aligned} \bar{X}_{\ell-1}(t_{n+1}) &= \bar{X}_{\ell-1}(t_n) + \nu_1 \mathcal{P}_{1,n} (a(\bar{X}_{\ell-1}(t_n)) \Delta t_\ell) + \nu_1 \mathcal{P}_{2,n} (a(\bar{X}_{\ell-1}(t_n)) \Delta t_\ell) \\ \bar{X}_\ell(t_{n+1}) &= \bar{X}_\ell(t_n) + \nu_1 \mathcal{Q}_{1,n} (a(\bar{X}_\ell(t_n)) \Delta t_\ell) + \nu_1 \mathcal{R}_{1,n} (a(\bar{X}_\ell(t_n + \Delta t_\ell)) \Delta t_\ell). \end{aligned}$$

Furthermore, by using the same reasoning of coupling strategy as in [3], we can show that for the first time interval $[t_n, t_n + \Delta t_\ell]$, we have

$$(2.4) \quad \begin{aligned} \bar{X}_{\ell-1}(t_n + \Delta t_\ell) &= \bar{X}_{\ell-1}(t_n) + \left(\mathcal{P}'_n (m_{\ell,n}^1 \Delta t_\ell) + \mathcal{P}''_n ((a(\bar{X}_{\ell-1}(t_n)) - m_{\ell,n}^1) \Delta t_\ell) \right) \nu_1 \\ \bar{X}_\ell(t_n + \Delta t_\ell) &= \bar{X}_\ell(t_n) + \left(\mathcal{P}'_n (m_{\ell,n}^1 \Delta t_\ell) + \mathcal{P}'''_n ((a(\bar{X}_\ell(t_n)) - m_{\ell,n}^1) \Delta t_\ell) \right) \nu_1, \end{aligned}$$

where $m_{\ell,n}^1 = \min(a(\bar{X}_\ell(t_n)), a(\bar{X}_{\ell-1}(t_n)))$, and $\mathcal{P}'_n, \mathcal{P}''_n, \mathcal{P}'''_n$ are conditionally independent Poisson rdvs.

For the time interval $[t_n + \Delta t_\ell, t_{n+1}]$, we have

$$(2.5) \quad \begin{aligned} \bar{X}_{\ell-1}(t_{n+1}) &= \bar{X}_{\ell-1}(t_n + \Delta t_\ell) + \left(\mathcal{Q}'_n (m_{\ell,n}^2 \Delta t_\ell) + \mathcal{Q}''_n ((a(\bar{X}_{\ell-1}(t_n)) - m_{\ell,n}^2) \Delta t_\ell) \right) \nu_1 \\ \bar{X}_\ell(t_{n+1}) &= \bar{X}_\ell(t_n + \Delta t_\ell) + \left(\mathcal{Q}'_n (m_{\ell,n}^2 \Delta t_\ell) + \mathcal{Q}'''_n ((a(\bar{X}_\ell(t_n + \Delta t_\ell)) - m_{\ell,n}^2) \Delta t_\ell) \right) \nu_1, \end{aligned}$$

where $m_{\ell,n}^2 = \min(a(\bar{X}_\ell(t_n + \Delta t_\ell)), a(\bar{X}_{\ell-1}(t_n)))$, and $\mathcal{Q}'_n, \mathcal{Q}''_n, \mathcal{Q}'''_n$ are conditionally independent Poisson rdvs.

(2.4) and (2.5) imply that

$$(2.6) \quad \begin{aligned} \bar{X}_\ell(t_{n+1}) - \bar{X}_{\ell-1}(t_{n+1}) &= \bar{X}_\ell(t_n) - \bar{X}_{\ell-1}(t_n) \\ &\quad + \nu_1 \left(\mathcal{P}'''_n (\Delta a_{\ell-1,n}^1 \Delta t_\ell) \mathbf{1}_{\Delta a_{\ell-1,n}^1 > 0} - \mathcal{P}''_n (-\Delta a_{\ell-1,n}^1 \Delta t_\ell) \mathbf{1}_{\Delta a_{\ell-1,n}^1 < 0} \right) \\ &\quad + \nu_1 \left(\mathcal{Q}'''_n (\Delta a_{\ell-1,n}^2 \Delta t_\ell) \mathbf{1}_{\Delta a_{\ell-1,n}^2 > 0} - \mathcal{Q}''_n (-\Delta a_{\ell-1,n}^2 \Delta t_\ell) \mathbf{1}_{\Delta a_{\ell-1,n}^2 < 0} \right), \end{aligned}$$

where $\Delta a_{\ell-1,n}^1 = a(\bar{X}_\ell(t_n)) - a(\bar{X}_{\ell-1}(t_n))$ and $\Delta a_{\ell-1,n}^2 = a(\bar{X}_\ell(t_n + \Delta t_\ell)) - a(\bar{X}_{\ell-1}(t_n))$.

In the following, we denote, for $0 \leq n \leq N_{\ell-1} - 1$ (note that $N_\ell = 2N_{\ell-1}$),

$$(2.7) \quad \begin{cases} \Delta a_{\ell,2n} = |\Delta a_{\ell-1,n}^1|, & \text{in } [t_n, t_n + \Delta t_\ell]. \\ \Delta a_{\ell,2n+1} = |\Delta a_{\ell-1,n}^2|, & \text{in } [t_n + \Delta t_\ell, t_{n+1}]. \end{cases}$$

Note that in (2.6), not only are $\mathcal{P}''_n, \mathcal{P}'''_n, \mathcal{Q}''_n, \mathcal{Q}'''_n$ rdvs, but $\Delta a_{\ell,2n}$ and $\Delta a_{\ell,2n+1}$ (defined in (2.7)) are also rdvs, because of their dependence on $\bar{X}_{\ell-1}(t_n)$, $\bar{X}_\ell(t_n)$, and $\bar{X}_\ell(t_n + \Delta t_\ell)$. Therefore, to derive some of the following formulas for analyzing our IS algorithm, we need to consider a sigma-algebra, \mathcal{F}_{n_ℓ} , with $0 \leq n_\ell \leq N_\ell - 1$, such that $\Delta a_{\ell,n_\ell}$, conditioned on \mathcal{F}_{n_ℓ} , is deterministic, *i.e.*,

$\Delta a_{\ell, n_\ell}$ is measurable with respect to \mathcal{F}_{n_ℓ} . This way, the only randomness being considered comes from the Poisson rdvs used for updating the states of $\bar{X}_\ell(t_{n+1})$ and $\bar{X}_{\ell-1}(t_{n+1})$. For this purpose, we consider for a fixed n_ℓ , \mathcal{F}_{n_ℓ} as the sigma algebra

$$(2.8) \quad \mathcal{F}_{n_\ell} := \sigma \left((\Delta a_{\ell, k})_{k=0, \dots, n_\ell} \right), \quad n_\ell = 0, \dots, N_\ell - 1.$$

In what follows, the terms $\{\Delta a_{\ell, n}\}_{n=0}^{N_\ell-1}$, defined in (2.7), will be denoted for the multi-channel case, by $\{\Delta a_{\ell, n}^j\}_{n=0}^{N_\ell-1}$, where $j \in \{1, \dots, J\}$ corresponds to the index of the reaction channel.

2.2 Characterization of the Optimal Change of Measure

It is known that, the optimal change of measure, π_ℓ , the one that achieves the minimum variance, satisfies

$$(2.9) \quad d\pi_0 \propto |g_0| d\mathbb{P}_0, \quad d\pi_\ell \propto |g_\ell - g_{\ell-1}| d\mathbb{P}_\ell.$$

Observe that the optimal measure, π_ℓ , removes the probability mass at zero, where most of \mathbb{P}_ℓ is concentrated due to catastrophic coupling (explained in Section 1.4.1). We emphasize that, in this work, we aim to perform a change of measure with respect to \mathbb{P}_ℓ , while keeping the single level measure \mathbb{P}_0 unchanged.

The minimum variance is given by

$$(2.10) \quad \begin{aligned} \text{Var}_{\pi_\ell} \left[(g_\ell - g_{\ell-1}) \frac{d\mathbb{P}_\ell}{d\pi_\ell} \right] &= (E_{\mathbb{P}_\ell} [|g_\ell - g_{\ell-1}|])^2 \left(1 - (E_{\pi_\ell} [\text{sgn}(g_\ell - g_{\ell-1})])^2 \right) \\ &= (E_{\mathbb{P}_\ell} [|g_\ell - g_{\ell-1}|])^2 \left(1 - (\pi_\ell(g_\ell - g_{\ell-1} > 0) - \pi_\ell(g_\ell - g_{\ell-1} < 0))^2 \right), \end{aligned}$$

where $\text{sgn}(\cdot)$ is the sign function.

Interestingly, using Theorem 3.2 in [5] in the context of the explicit TL scheme for pure jump processes, we conclude that $E_{\mathbb{P}_\ell} [|g_\ell - g_{\ell-1}|] = \mathcal{O}(\Delta t_\ell)$ for any Lipschitz function g . Therefore, we clearly observe that the optimal IS improves the strong convergence rate, and hence leads to the optimal complexity rate of the MLMC estimator (see Theorem 1.1).

Unfortunately, it is unfeasible to sample from π_ℓ ; therefore, our goal in the following sections is to propose a practical IS algorithm with a sub-optimal change of measure, $\bar{\pi}_\ell$.

3 Main Results

Our analysis and theoretical estimates in Section 4, and numerical experiments in Section 5 show that

1. For $\ell = 1, \dots, L$, and $g_\ell := g(\bar{\mathbf{X}}_\ell)$: the change of measure is performed at each time step, for $0 \leq n \leq N_\ell - 1$, by going forward in time, and is only applied when

$$(3.1) \quad \text{i) } j \in \mathcal{J}_1 := \{1 \leq j \leq J; \quad g(\mathbf{X} + \boldsymbol{\nu}_j) \neq g(\mathbf{X})\} \quad \& \quad \text{ii) } \Delta a_{\ell, n}^j \neq 0 \quad \& \quad \text{iii) } \Delta g_\ell(t_n) = 0$$

where $\Delta g_\ell := g_\ell - g_{\ell-1}$.

2. If (3.1) is fulfilled: instead of using $\Delta a_{\ell,n}^j \Delta t_\ell$ in (2.7), we propose to use $\lambda_{\ell,n}^j \Delta t_\ell$, with $\lambda_{\ell,n}^j$ is given by

$$(3.2) \quad \lambda_{\ell,n}^j = c_\ell \Delta a_{\ell,n}^j = \Delta t_\ell^{-\delta} \Delta a_{\ell,n}^j, \quad 0 < \delta < 1,$$

where δ is a scale parameter in our IS algorithm.

3. We show that our proposed method (MLMC with IS) significantly reduces the kurtosis at the deep levels of MLMC (small Δt_ℓ) (see Theorem 4.1 and the numerical experiments in Section 5), and also improves the strong convergence rate from $\beta = 1$, for the standard case (without IS), to $\beta = 1 + \delta$, where $0 < \delta < 1$ is a user-selected parameter in our IS algorithm (see Theorem 4.2, and the numerical experiments in Section 5). Due to Theorem 1.1, and given a pre-selected tolerance, TOL, this results in an improvement of the complexity from $\mathcal{O}(\text{TOL}^{-2} \log(\text{TOL})^2)$, in the standard case, to the optimal complexity, *i.e.*, $\mathcal{O}(\text{TOL}^{-2})$. These improvements come with a negligible additional cost since we show in Section 4.4 that $W_{\ell,\text{sample}}^{\text{without IS}} \approx W_{\ell,\text{sample}}^{\text{with IS}}$ ($W_{\ell,\text{sample}}$ denotes the average cost of simulating coupled MLMC paths at level ℓ). We show a summary of these results in Table 3.1; see Sections 4 and 5 for more details.

Quantity of Interest	MLMC Without IS (standard case)	MLMC With IS ($0 < \delta < 1$)
κ_ℓ	$\mathcal{O}(\Delta t_\ell^{-1})$	$\mathcal{O}(\Delta t_\ell^{\delta-1})$
V_ℓ	$\mathcal{O}(\Delta t_\ell)$	$\mathcal{O}(\Delta t_\ell^{1+\delta})$
$W_{\ell,\text{sample}}$	$\approx 2 \times J \times C_p \times \Delta t_\ell^{-1}$	$\approx 2 \times J \times C_p \times \Delta t_\ell^{-1}$
$\text{Work}_{\text{MLMC}}$	$\mathcal{O}(\text{TOL}^{-2} \log(\text{TOL})^2)$	$\mathcal{O}(\text{TOL}^{-2})$

Table 3.1: Main results for the comparison of MLMC combined with our IS algorithm, and standard MLMC. κ_ℓ denotes the kurtosis of the coupled MLMC paths at level ℓ . V_ℓ denotes the variance of the coupled MLMC paths at level ℓ . C_p is the cost of generating one Poisson rrv.

4 Construction of the IS Measure and Convergence Estimates

4.1 Construction of the IS Measure: The One-Dimensional Case

We start with the one-dimensional case (only one species), where the number of reactions is ($J = 1$). Instead of using $\Delta a_{\ell,n} \Delta t_\ell$ as the rate parameter of the Poisson rrvs used in each time step to update the states of the coupled paths ((2.4), (2.5)) where $\Delta a_{\ell,n}$ is given by (2.7), we suggest using $\lambda_{\ell,n} \Delta t_\ell$, with the parameter $\lambda_{\ell,n}$, which will be determined given some constraints that we impose to ensure that our change of measure is i) reducing the kurtosis of the MLMC estimator at the deep levels, ii) reducing the variance of the MLMC levels and increasing the strong convergence rate. In the following, we denote $g_\ell := g(\bar{\mathbf{X}}_\ell)$, and $\Delta g_\ell := g_\ell - g_{\ell-1}$, for $\ell = 1, \dots, L$.

The change of measure is performed at each time step by going forward in time, and is only applied when it is needed, *i.e.*, we impose the following condition for applying the change of measure

$$(4.1) \quad \Delta a_{\ell,n} \neq 0 \quad \& \quad \Delta g_\ell(t_n) = 0, \quad 0 \leq n \leq N_\ell - 1, \quad \ell = 1, \dots, L.$$

Condition (4.1) is motivated by the fact that i) we need to change the measure only in cases where the coupled paths at the n th time step are equal and ii) for cases where the rates of the Poisson rdvs are non zero, so we do not have the issue of the likelihood being equal to zero.

Whenever (4.1) holds, the change of measure is given by changing the rate of the Poisson rdvs (see (2.6) and (2.7)) in the tau-leap approximation from $\Delta a_{\ell,n} \Delta t_\ell$ to $\lambda_{\ell,n} \Delta t_\ell$. Hence, the conditional likelihood is then given by the ratio between the probability mass functions of two Poisson rdvs with rates $\Delta a_{\ell,n} \Delta t_\ell$ and $\lambda_{\ell,n} \Delta t_\ell$. Through a simple computation, this leads to

$$\begin{aligned} L_{\ell,n} &= \frac{e^{-\Delta a_{\ell,n} \Delta t_\ell}}{e^{-\lambda_{\ell,n} \Delta t_\ell}} \left(\frac{\Delta a_{\ell,n}}{\lambda_{\ell,n}} \right)^{k_n}, \quad n \in \mathcal{I}_\ell^s \\ (4.2) \quad &= e^{-\Delta t_\ell (\Delta a_{\ell,n} - \lambda_{\ell,n})} \left(\frac{\Delta a_{\ell,n}}{\lambda_{\ell,n}} \right)^{k_n}, \end{aligned}$$

where k_n is the number of jumps that occurs at the n th time step where we apply the change of measure, and \mathcal{I}_ℓ^s is the random set including the time steps at level ℓ where we simulate the Poisson rdvs under the new measure.

Thus, across one path, the likelihood ratio is given by

$$(4.3) \quad L_\ell = e^{-\Delta t_\ell \sum_{n \in \mathcal{I}_\ell^s} (\Delta a_{\ell,n} - \lambda_{\ell,n})} \prod_{n \in \mathcal{I}_\ell^s} \left(\frac{\Delta a_{\ell,n}}{\lambda_{\ell,n}} \right)^{k_n}.$$

Furthermore, if we impose that $\lambda_{\ell,n} = c_\ell \Delta a_{\ell,n}$ then we obtain

$$(4.4) \quad L_\ell = \left(e^{(c_\ell - 1) \Delta t_\ell \sum_{n \in \mathcal{S}} \Delta a_{\ell,n}} \right) \left(c_\ell^{-\sum_{n \in \mathcal{S}} k_n} \right).$$

We note that imposing $\lambda_{\ell,n} = c_\ell \Delta a_{\ell,n}$ can be motivated by the fact that we want to keep the same physical structure of the rate of the Poisson process driving the state changes, *i.e.*, depending on $\Delta a_{\ell,n}$. However, we try to introduce a scaled constant c_ℓ that depends on Δt_ℓ so that we reduce the probability of having $\Delta g_\ell(T) = 0$, under the new measure. A reasonable choice of c_ℓ is given by

$$(4.5) \quad c_\ell = \Delta t_\ell^{-\delta},$$

where $\delta > 0$ is the scale parameter to be determined. Note that the case $\delta = 0$ is similar to the case of using the old measure in all time steps.

Remark 4.1. Observe that for $\delta \in (0, 1)$ and $g(x) = x$, $x \in \mathbb{R}$, we have $\bar{\pi}_\ell(|\Delta \bar{X}_\ell(T)| = 0)$ is still approaching 1 as Δt_ℓ decreases, but compared to the initial situation (without IS), we decrease the rate of convergence with respect to Δt_ℓ (compare Figure 5.3, for the case without IS, and Figure 5.8 for the case with IS with $\delta = \frac{3}{4}$).

4.2 Construction of the IS Measure:: The Multi-Channels and High Dimensional States Case

Extending our method to a higher dimension in the number of reaction channels, J , and in the state vector \mathbf{X} is straightforward with slight modifications. We first define the set \mathcal{J}_1 as

$$\mathcal{J}_1 = \{1 \leq j \leq J; \quad g(\mathbf{X} + \boldsymbol{\nu}_j) \neq g(\mathbf{X})\}.$$

In the multi-channel case, we are only interested in changing the measure for reactions whose stoichiometric vector, $\boldsymbol{\nu}_j$, changes the state of the quantity of interest, *i.e.*, for reactions with index $j \in \mathcal{J}_1$. In Algorithm 4.1, we summarize our methodology for simulating two coupled explicit TL paths with IS.

Algorithm 4.1 Simulates two coupled explicit TL paths with IS, and computes the likelihood ratio.

```

1: Fix  $\Delta t_\ell > 0$  and set  $\Delta t_{\ell-1} = 2 \times \Delta t_\ell$ .
2: Set  $\mathbf{Z}_\ell(0) = \mathbf{Z}_{\ell-1}(0) = \mathbf{x}_0$ ,  $t_\ell = t_{\ell-1} = 0$ ,  $n = 0$ .
3: Set  $c_\ell = \Delta t_\ell^{-\delta}$ ,  $\delta \in (0, 1)$ 
4: while  $t_\ell < T$  do
5:    $n = n + 1$ 
6:   for  $j=1$  to  $J$  do
7:     if  $(a_j(\mathbf{Z}_\ell(t_\ell)) \neq a_j(\mathbf{Z}_{\ell-1}(t_{\ell-1})) \ \& \ g(\mathbf{Z}_\ell(t_\ell)) = g(\mathbf{Z}_{\ell-1}(t_\ell)) \ \& \ j \in \mathcal{J}_1)$  then
8:        $A_{3(j-1)+1} = \min(a_j(\mathbf{Z}_\ell(t_\ell)), a_j(\mathbf{Z}_{\ell-1}(t_{\ell-1})))$ 
9:        $A_{3(j-1)+2} = c_\ell (a_j(\mathbf{Z}_\ell(t_\ell)) - A_{3(j-1)+1})$ 
10:       $A_{3(j-1)+3} = c_\ell (a_j(\mathbf{Z}_{\ell-1}(t_{\ell-1})) - A_{3(j-1)+1})$ 
11:      Compute  $L_{\ell,n}$  using (4.2) and update the likelihood terms,  $L_\ell^j$  and  $L_\ell$  using (4.7) and
      (4.8).
12:     else
13:        $A_{3(j-1)+1} = \min(a_j(\mathbf{Z}_\ell(t_\ell)), a_j(\mathbf{Z}_{\ell-1}(t_{\ell-1})))$ 
14:        $A_{3(j-1)+2} = a_j(\mathbf{Z}_\ell(t_\ell)) - A_{3(j-1)+1}$ 
15:        $A_{3(j-1)+3} = a_j(\mathbf{Z}_{\ell-1}(t_{\ell-1})) - A_{3(j-1)+1}$ 
16:        $\Lambda_{3(j-1)+1} = \text{Poisson}(A_{3(j-1)+1} \Delta t_\ell)$ 
17:        $\Lambda_{3(j-1)+2} = \text{Poisson}(A_{3(j-1)+2} \Delta t_\ell)$ 
18:        $\Lambda_{3(j-1)+3} = \text{Poisson}(A_{3(j-1)+3} \Delta t_\ell)$ 
19:       State updating
      i) Set  $\boldsymbol{\Gamma}_\ell = \boldsymbol{\nu} \otimes [1 \ 1 \ 0]$  and  $\boldsymbol{\Gamma}_{\ell-1} = \boldsymbol{\nu} \otimes [1 \ 0 \ 1]$  ( $A \otimes B$  refers to the Kronecker product of the
      matrices  $A$  and  $B$ ).
      ii) Update  $\mathbf{Z}_\ell(t_\ell + \Delta t_\ell) = \mathbf{Z}_\ell(t_\ell) + \Delta t_\ell \boldsymbol{\Gamma}_\ell \boldsymbol{\Lambda}$ 
      iii) Update  $\mathbf{Z}_{\ell-1}(t_\ell + \Delta t_\ell) = \mathbf{Z}_{\ell-1}(t_\ell) + \Delta t_\ell \boldsymbol{\Gamma}_{\ell-1} \boldsymbol{\Lambda}$ 
20:   if  $(n \bmod 2) = 0$  then  $t_{\ell-1} = t_{\ell-1} + \Delta t_{\ell-1}$ 
21:    $t_\ell = t_\ell + \Delta t_\ell$ 

```

We consider a number of reactions $J > 1$, $\mathbf{X} \in \mathbb{N}^d$, $d \geq 1$ and $g : \mathbb{R}^d \rightarrow \mathbb{R}$. Hereafter, we denote by $\{\nu_{j,i}\}_{j=1}^J$ the coordinates in the stoichiometric vectors, $\{\boldsymbol{\nu}_j\}_{j=1}^J$, corresponding to the state change of the i th species. For a fixed $0 \leq n \leq N_\ell - 1$, we define \mathcal{F}_n to be the sigma algebra given by

$$(4.6) \quad \mathcal{F}_n := \sigma \left(\left(\Delta a_{\ell,k}^j \right)_{j=1,\dots,J; k=0,\dots,n} \right), \quad n = 0, \dots, N_\ell - 1.$$

The likelihood ratio for each reaction channel $j \in \mathcal{J}_1$ has a similar expression to (4.4), and is given

by

$$(4.7) \quad L_\ell^j = \left(e^{(c_\ell-1)\Delta t_\ell \sum_{n \in \mathcal{I}_{\ell,j}^s} \Delta a_{\ell,n}^j} \right) \left(c_\ell^{-\sum_{n \in \mathcal{I}_{\ell,j}^s} k_n^j} \right), \quad j \in \mathcal{J}_1,$$

where k_n^j is the number of jumps associated with the j th reaction channel that occurs at the n th time step where we apply the change of measure, and $\mathcal{I}_{\ell,j}^s$ is the random set including the time steps at level ℓ , where we simulate the Poisson rdvs under the new measure for the j th reaction channel.

Thus, across one path, the likelihood ratio is given by

$$(4.8) \quad L_\ell = \prod_{j \in \mathcal{J}_1} L_\ell^j = \left(e^{(c_\ell-1)\Delta t_\ell \sum_{j \in \mathcal{J}_1} \sum_{n \in \mathcal{I}_{\ell,j}^s} \Delta a_{\ell,n}^j} \right) \left(c_\ell^{-\sum_{j \in \mathcal{J}_1} \sum_{n \in \mathcal{I}_{\ell,j}^s} k_n^j} \right).$$

Similarly to Section 4.1, we choose c_ℓ to be given by (4.5), with $\delta > 0$. Remark 4.1 holds for the high dimensional case. In particular, compare Figures 5.5 and 5.7, for the case without IS, and Figures 5.11 and 5.14 for the case using IS with $\delta = \frac{3}{4}$, for $g(\mathbf{X}) = X^{(i)}$, i.e., the projection on the i th coordinate of the state vector \mathbf{X} .

4.3 Convergence Estimates of MLMC combined with IS

In this section, we aim to derive convergence estimates of the kurtosis and the variance. We start by stating the main two assumptions (Assumptions 4.1 and 4.2), needed to derive the main results in this section. For the ease of presentation, we consider $g(\mathbf{X}) = X^{(i)}$, the projection on the i th coordinate of the state vector \mathbf{X} .

Assumption 4.1. For a small Δt_ℓ , and conditioning on $\mathcal{F}_{N_\ell-1}$ and $(\mathcal{I}_{\ell,j}^s = \mathcal{S}_j)_{j \in \mathcal{J}_1}$, we denote, for $j \in \mathcal{J}_1$, $K_j = \sum_{n \in \mathcal{S}_j} k_n^j$, and we assume that, for $0 \leq \delta < 1$,

(a) for all $\bar{\mathbf{K}} \in \mathbb{N}^{\#\mathcal{J}_1}$ such that $\sum_{j \in \mathcal{J}_1} \nu_{j,i} \bar{K}_j \neq 0$, we have

$$\frac{\bar{\pi}_\ell \left(|\Delta g_\ell(T)| = \left| \sum_{j \in \mathcal{J}_1} \nu_{j,i} \bar{K}_j \right|, \cap_{j \in \mathcal{J}_1} \{K_j = \bar{K}_j\}; \left(\mathcal{F}_{N_\ell-1}, (\mathcal{I}_{\ell,j}^s = \mathcal{S}_j)_{j \in \mathcal{J}_1} \right) \right)}{\sum_{j \in \mathcal{J}_1} \bar{\pi}_\ell \left(|\Delta g_\ell(T)| = |\nu_{j,i}|, \{K_j = 1\} \cap_{q \neq j} \{K_q = 0\}; \left(\mathcal{F}_{N_\ell-1}, (\mathcal{I}_{\ell,j}^s = \mathcal{S}_j)_{j \in \mathcal{J}_1} \right) \right)} \leq 1.$$

(b) for all $q \geq 1$, there exists $\eta_{q,\ell} > 0$ such that,

$$\bar{\pi}_\ell \left\{ |\Delta g_\ell(T)| = q; \left(\mathcal{F}_{N_\ell-1}, (\mathcal{I}_{\ell,j}^s = \mathcal{S}_j)_{j \in \mathcal{J}_1} \right) \right\} \leq \eta_{q,\ell} \Delta t_\ell^{(1-\delta)q}, \quad \text{with } \frac{\eta_{q+1,\ell}}{\eta_{q,\ell}} \leq \eta,$$

with η independent of ℓ and q .

(c) for all $j \in \mathcal{J}_1$ there exist a single $n_j^* \in \mathcal{S}_j$ such that

$$\bar{\pi}_\ell \left\{ |\Delta g_\ell(T)| = |\nu_{j,i}|, \{K_j = 1\} \cap_{q \neq j} \{K_q = 0\}; \left(\mathcal{F}_{N_\ell-1}, (\mathcal{I}_{\ell,j}^s = \mathcal{S}_j)_{j \in \mathcal{J}_1} \right) \right\} = e^{-\Delta t_\ell^{1-\delta} \Delta a_{\ell,n_j^*}^j} \left(\Delta t_\ell^{1-\delta} \Delta a_{\ell,n_j^*}^j \right) (1 + o(1)).$$

Assumption 4.2. *There exists $\ell_0 \geq 0$ such that for all $\ell \geq \ell_0$, we have*

$$0 < C_1 \leq \sum_{j \in \mathcal{J}_1} \mathbb{E}_{\pi_\ell} \left[e^{-\Delta a_{\ell, n_j}^j} \Delta a_{\ell, n_j}^j \right] \leq \mathbb{E}_{\pi_\ell} \left[e^{\sum_{j \in \mathcal{J}_1} \sum_{n \in \mathcal{I}_{\ell, j}^s} \Delta a_{\ell, n_j}^j} \right] \leq C_2 < \infty,$$

where C_1, C_2 are independent of ℓ , and n_j^* are defined in Assumption 4.1 (c).

We emphasize that Assumption 4.1 (c) is motivated by our numerical observations, which suggest that for small values of Δt_ℓ , we sample at most one single step using our IS algorithm, which separates the two paths (see Figures B.1, B.2 and B.3 in Appendix B). Furthermore, by observing that $\Delta a_{\ell, n}^j = \mathcal{O}(1)$, $\forall j \in \mathcal{J}_1$, Assumption 4.2 is motivated by our numerical observations (see Figures 4.1a and 4.1b), which show that $\mathbb{E} \left[\sum_{j \in \mathcal{J}_1} \# \mathcal{I}_{\ell, j}^s \right] = \mathcal{O}(1)$.

Now, we state the main results of this section through Theorems 4.1 and 4.2. The proof of these theorems are identical to the one dimensional proofs (one species and one reaction ($J = 1$)) with slight differences. Consequently, for ease of presentation, we present in Appendix A the one dimensional proofs. The key result for these proofs is Lemma 4.1 which is proven in Appendix A. In the following and without loss of generality, we also assume that $|\nu_1| = 1$.

lemma 4.1 (Conditional L^p moments estimates). *Let $J = 1$, $p \geq 1$ and $0 \leq \delta < 1$, and suppose that Assumptions 4.1 and 4.2 hold, then, for $\Delta t_\ell \rightarrow 0$, we have*

$$(4.9) \quad \mathbb{E}_{\pi_\ell} [|\Delta g_\ell|^p(T) L_\ell^p; (\mathcal{F}_{N_\ell-1}, \mathcal{I}_\ell^s = \mathcal{S})] = \Delta t_\ell^{(p-1)\delta+1} (\Delta a_{\ell, n^*}) e^{p(\Delta t_\ell^{1-\delta} - \Delta t_\ell) \sum_{n \in \mathcal{S}} \Delta a_{\ell, n}} e^{-(\Delta t_\ell^{1-\delta} \Delta a_{\ell, n^*})} (1 + h_{p, \ell}),$$

such that $h_{p, \ell} \xrightarrow{\Delta t_\ell \rightarrow 0} 0$.

Remark 4.2. *Note that for $J \geq 1$, Lemma 4.1 is extended to the multi-channel case by expressing the right-hand side of 4.9 as a summation over the set \mathcal{J}_1 of similar terms but involving $\Delta a_{\ell, n}^j$ instead of $\Delta a_{\ell, n}$. These terms correspond to only one jump occurring under the new measure and due to the firing of only one reaction channel $j \in \mathcal{J}_1$.*

Finally a further assumption (Assumption 4.3) is needed to prove Theorems 4.1 and 4.2

Assumption 4.3. *For a sufficiently large ℓ , we assume that there exists a constant C_p , independent of ℓ , such that $h_{p, \ell}$ in Lemma 4.1 fulfills $\mathbb{E}_{\pi_\ell} [h_{p, \ell}^2] \leq C_p < \infty$.*

Theorem 4.1 shows that the kurtosis at level ℓ of the MLMC estimator combined with our IS algorithm, κ_ℓ , is $\mathcal{O}(\Delta t_\ell^{\delta-1})$.

Theorem 4.1. *Let $J \geq 1$ and let us denote $Y_\ell := \Delta g_\ell(T) L_\ell$. Suppose that Assumptions 4.1, 4.2 and 4.3 hold. Then, for $0 \leq \delta < 1$ and $\Delta t_\ell \rightarrow 0$, we have*

$$(4.10) \quad \kappa_\ell := \frac{\mathbb{E}_{\pi_\ell} [(Y_\ell - \mathbb{E}_{\pi_\ell} [Y_\ell])^4]}{(\text{Var}_{\pi_\ell} [Y_\ell])^2} = \mathcal{O}(\Delta t_\ell^{\delta-1}).$$

Theorem 4.1 clearly shows the effect seen for the limiting case $\delta = 0$ where we do not apply the IS algorithm and thus, the kurtosis κ_ℓ increases at a rate of Δt_ℓ^{-1} . Compared to the case without IS, we reduce the kurtosis by a factor of $\Delta t_\ell^{-\delta}$. Theorem 4.1 is confirmed by our numerical experiments in Section 5.

Let us fix $0 \leq \delta < 1$. We show in Theorem 4.2 that the strong convergence rate is $\beta = \delta + 1$.

Theorem 4.2. *Let $0 \leq \delta < 1$ and $J \geq 1$ and let us denote $Y_\ell := \Delta g_\ell(T)L_\ell$. Suppose that Assumptions 4.1, 4.2 and 4.3 hold. Then, for $\Delta t_\ell \rightarrow 0$, we have*

$$\text{Var}_{\pi_\ell}[Y_\ell] = \mathcal{O}\left(\Delta t_\ell^{1+\delta}\right).$$

The result in Theorem 4.2 is confirmed by the numerical experiments in Section 5, which demonstrate that our IS algorithm improves the strong convergence rate from $\beta = 1$ (see Figures 5.2, 5.4, and 5.6) to $\beta = 1 + \delta$ with $\delta > 0$ (see Figures 5.9 and 5.10 for Example 5.1, 5.12 and 5.13 for Example 5.2, and Figures 5.15 and 5.16 for Example 5.3) for the case with IS. Due to Theorem 1.1, and given that $\gamma = 1$ (work rate) for both cases, with and without IS, we improve the complexity of the MLMC method from $\mathcal{O}(\text{TOL}^{-2} \log(\text{TOL})^2)$ for the case without IS to the optimal complexity, *i.e.*, $\mathcal{O}(\text{TOL}^{-2})$, for the case with IS, where TOL is a pre-selected tolerance.

Remark 4.3 (More general observable g). *For ease of presentation, we formulate our assumptions and show our proofs for an observable g in the class of projections. However, our results can be easily extended to include linear maps, and linear combination of indicator functions.*

4.4 Cost Analysis

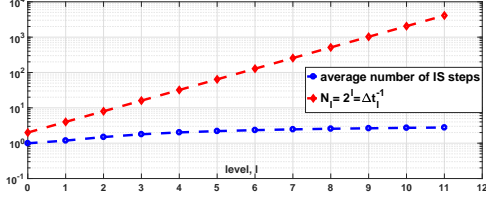
In this section, we analyze briefly the computational costs when using MLMC with our IS technique compared to standard MLMC, in the context of SRNs. Let M_ℓ denote the number of samples at level ℓ , and $W_{\ell,\text{sample}}$ the expected cost per sample path at level ℓ . Observe that the expected computational cost of the MLMC estimator is given by

$$W_{\text{MLMC}} := \sum_{\ell=0}^L M_\ell W_{\ell,\text{sample}},$$

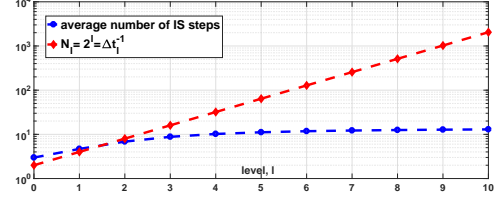
If we denote by $W_{\ell,\text{sample}}^{\text{with IS}}$ and $W_{\ell,\text{sample}}^{\text{without IS}}$ the expected costs of simulating one sample path at level ℓ with and without IS, respectively, then we have

$$(4.11) \quad \begin{aligned} W_{\ell,\text{sample}}^{\text{without IS}} &\approx 2 \times J \times C_p \times \Delta t_\ell^{-1} \\ W_{\ell,\text{sample}}^{\text{with IS}} &\approx 2 \times J \times C_p \times \Delta t_\ell^{-1} + \underbrace{C_{\text{lik}}}_{\ll C_p} \times \underbrace{\sum_{j \in \mathcal{J}_1} \overline{\# \mathcal{I}_{\ell,j}^s}}_{\ll \Delta t_\ell^{-1}} \approx W_{\ell,\text{sample}}^{\text{without IS}}, \end{aligned}$$

where C_p is the cost of generating one Poisson rrv, C_{lik} is the cost of computing the likelihood ratio, and $\overline{\sum_{j \in \mathcal{J}_1} \# \mathcal{I}_{\ell,j}^s}$ is the average number of time steps at level ℓ , where we simulate under the new measure the j th reaction channel. We note that the inequality $\overline{\sum_{j \in \mathcal{J}_1} \# \mathcal{I}_{\ell,j}^s} \ll \Delta t_\ell^{-1}$ is motivated and justified by the construction of our IS algorithm, where IS is only applied a few times across each simulated path. This is also confirmed by Figure 4.1. Furthermore, we refer to Figure 4.2 for evidence of the observation made by (4.11).

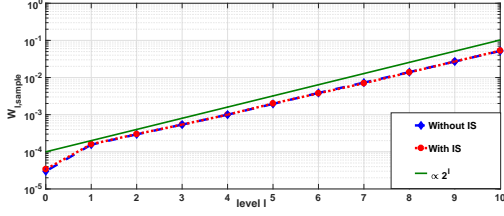


(a) Example 5.1.

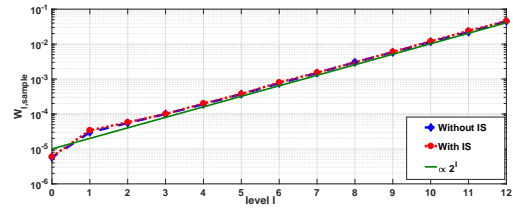


(b) Example 5.3.

Figure 4.1: Average number of time steps for different MLMC levels, $\overline{\sum_{j \in \mathcal{J}_1} \# \mathcal{I}_{\ell,j}^s}$, with IS (with $\delta = \frac{3}{4}$), with 10^5 samples. This Figure shows that $\overline{\sum_{j \in \mathcal{J}_1} \# \mathcal{I}_{\ell,j}^s} = \mathcal{O}(1) \ll \Delta t_\ell^{-1}$.



(a) Example 5.2.

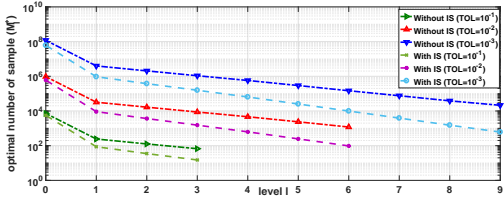


(b) Example 5.3.

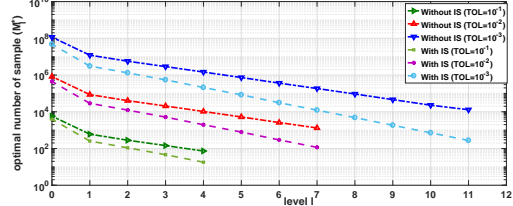
Figure 4.2: Comparison of the average cost per sample path per level (in CPU time and estimated with 10^6 samples). MLMC combined with IS (with $\delta = \frac{3}{4}$) has the same average cost per sample path per level, as standard MLMC.

Furthermore, if we denote by $V_\ell = \text{Var}[g_\ell - g_{\ell-1}]$, then from our analysis in Section 4.2, and our numerical experiments in Section 5, it is shown that $V_\ell^{\text{with IS}} \ll V_\ell^{\text{without IS}}$ implying that $\Rightarrow M_\ell^{\text{with IS}} \ll M_\ell^{\text{without IS}}$ (see Figure 4.3).

Therefore, we conclude that combining our pathwise IS with the MLMC estimator not only improves its robustness and convergence behavior, but also significantly reduces the cost.



(a) Example 5.2.



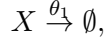
(b) Example 5.3.

Figure 4.3: Comparison of the optimal number of samples per level, using (1.8), for different pre-selected tolerances TOL for the MLMC estimator. For a fixed TOL, the optimal number of samples per level of MLMC with IS (with $\delta = \frac{3}{4}$) is significantly smaller than the one of MLMC without IS.

5 Numerical Experiments

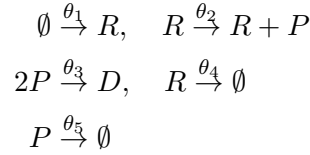
In the following, we illustrate the main benefits of the MLMC-based method, when used in combination with our IS algorithm (explained in Section 4), compared to the standard MLMC used in [3]. We consider three different examples of SRNs, given by Examples 5.1, 5.2, and 5.3, where we use the MLMC method to estimate $E[g(\mathbf{X}(T))]$, where \mathbf{X} is the state vector representing the counting number of each species in the system, $g : \mathbb{R}^d \rightarrow \mathbb{R}$ is a given scalar observable of \mathbf{X} , and $T > 0$ is a user-selected final time. We note that our numerical results were obtained using an Intel(R) Xeon(R) CPU E5-2680 architecture. Furthermore, the computer code is written in the MATLAB programming language (version R2019a), and it can be downloaded from https://github.com/hammouc/MLMC_IS_SRNs.

Example 5.1 (Decay example). *This model has one reaction,*



with $\theta_1 = 1$, $T = 1$, and $X_0 = 10$. The stoichiometric scalar $\nu = -1$ and the propensity function $a(x) = \theta_1 x$. The quantity of interest in this example is $E[X(T)]$.

Example 5.2 (Gene transcription and translation [3]). *This model has five reactions,*

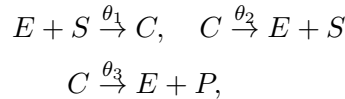


with $\boldsymbol{\theta} = (25, 10^3, 0.001, 0.1, 1)$, $T = 1$, $\mathbf{X}(t) = (R(t), P(t), D(t))$ and $\mathbf{X}_0 = (0, 0, 0)$. The stoichiometric matrix and the propensity functions are given by

$$\boldsymbol{\nu} = \begin{pmatrix} 1 & 0 & 0 \\ 0 & 1 & 0 \\ 0 & -2 & 1 \\ -1 & 0 & 0 \\ 0 & -1 & 0 \end{pmatrix}, \quad a(\mathbf{X}) = \begin{pmatrix} \theta_1 \\ \theta_2 R \\ \theta_3 P(P-1) \\ \theta_4 R \\ \theta_5 P \end{pmatrix}$$

The quantity of interest is $E[X^{(1)}(T)]$. We note that the choice of $X^{(1)}$ as the target species was determined by selecting the i th species with the highest probability of having $\overline{X}_\ell^{(i)}(T) - \overline{X}_{\ell-1}^{(i)}(T) = 0$ on the deep levels, resulting in the most severe catastrophic coupling explained in Section 1.4.1. In this example, the coarsest level of the MLMC estimator is $L_0 = 2$.

Example 5.3 (Michaelis-Menten enzyme kinetics [37]). *The catalytic conversion of a substrate, S , into a product, P , via an enzymatic reaction involving enzyme, E . This is described by Michaelis-Menten enzyme kinetics with three reactions,*



with $\boldsymbol{\theta} = (0.001, 0.005, 0.01)$, $T = 1$, $\mathbf{X}(t) = (E(t), S(t), C(t), P(t))$ and $\mathbf{X}_0 = (100, 100, 0, 0)$. The stoichiometric matrix and the propensity functions are given by

$$\boldsymbol{\nu} = \begin{pmatrix} -1 & -1 & 1 & 0 \\ 1 & 1 & -1 & 0 \\ 1 & 0 & -1 & 1 \end{pmatrix}, \quad a(\mathbf{X}) = \begin{pmatrix} \theta_1 ES \\ \theta_2 C \\ \theta_3 C \end{pmatrix}$$

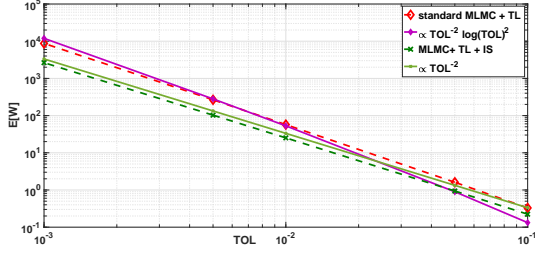
The quantity of interest in this example is $E[X^{(3)}(T)]$.

We show in Table 5.1 the summarized results, related to the convergence rates, for the different scenarios without/with IS, and for the different examples that we consider in our numerical experiments. We also show several cases depending on the parameter, δ , used in the IS algorithm. From this table, we can see that our IS algorithm, besides dramatically reducing the kurtosis, improves the strong convergence rates from 1 to $1 + \delta$, which then improves the total complexity of the MLMC estimator from $\mathcal{O}(\text{TOL}^{-2} \log(\text{TOL}^2))$ to $\mathcal{O}(\text{TOL}^{-2})$, where TOL is a pre-selected tolerance. This improvement is confirmed by Figure 5.1, which shows that MLMC, when used in combination with our IS algorithm, achieves the same numerical complexity, $\mathcal{O}(\text{TOL}^{-2})$ as MC with an exact method (SSA), but with a significantly smaller constant. The detailed convergence plots for each example are presented in Sections 5.1 and 5.2.

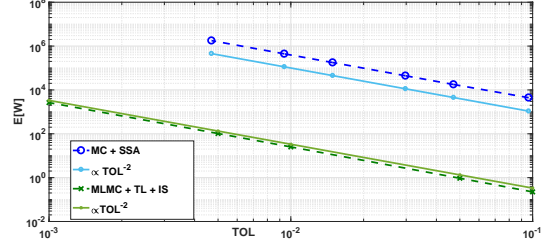
Figure 5.1 illustrates the improvement of the complexity rate compared to standard MLMC. For both examples 5.2 and 5.3, MLMC, when used in combination with our IS algorithm, significantly outperforms the standard MLMC. In particular, to achieve a desired accuracy of $\text{TOL} = 10^{-3}$ in example 5.2, MLMC with IS ($\delta = \frac{3}{4}$) requires around 30% of the total work (in CPU time) of MLMC without IS. To achieve the same accuracy in example 5.3, MLMC with IS ($\delta = \frac{3}{4}$) requires around 18% of the total work of MLMC without IS. We note that the different parameters of the MLMC estimator such as i) the coarsest level, L_0 , the deepest level, L , and the optimal number of samples $\{M_\ell\}_{\ell=L_0}^L$, were selected using a similar procedure to the procedure in [27].

Example	α	β	γ	κ_L
Example 5.1 without IS	1.04	1.03	1	2191
Example 5.1 with IS ($\delta = 1/4$)	1.04	1.27	1	275
Example 5.1 with IS ($\delta = 1/2$)	1.04	1.57	1	34.2
Example 5.1 with IS ($\delta = 3/4$)	1.04	1.93	1	5.1
Example 5.2 without IS	1	0.99	1	3290
Example 5.2 with IS ($\delta = 1/4$)	1	1.23	1	409
Example 5.2 with IS ($\delta = 1/2$)	1	1.47	1	50
Example 5.2 with IS ($\delta = 3/4$)	1	1.72	1	5.8
Example 5.3 without IS	1.02	1.03	1	1130
Example 5.3 with IS ($\delta = 1/4$)	1.02	1.26	1	208
Example 5.3 with IS ($\delta = 1/2$)	1.02	1.5	1	36.7
Example 5.3 with IS ($\delta = 3/4$)	1.03	1.75	1	5.9

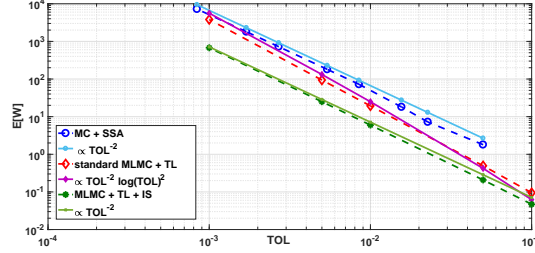
Table 5.1: Comparison of convergence rates (α , β , γ), and the kurtosis at the deepest levels of MLMC, κ_L , for the different examples with and without the IS algorithm. α, β, γ are the estimated rates of weak convergence, strong convergence and computational work, respectively, with a number of samples $M = 10^6$. The detailed convergence plots are presented in Sections 5.1 and 5.2.



(a) Example 5.2.



(b) Example 5.2



(c) Example 5.3.

Figure 5.1: Comparison of the numerical complexity of the different methods i) MC with SSA, ii) standard MLMC with TL, and iii) MLMC with TL in combination with IS ($\delta = \frac{3}{4}$). MLMC combined with our IS algorithm achieves the same numerical complexity, $\mathcal{O}(\text{TOL}^{-2})$, as MC with an exact method (SSA), but with a significantly smaller constant. On the other hand, MLMC in combination with IS algorithm significantly outperforms standard MLMC.

5.1 Numerical Results of MLMC Without IS

In Figures 5.2, 5.4 and 5.6 , we show the convergence plots for the MLMC method without IS for Examples 5.1, 5.2 and 5.3, respectively. In these figures, and specifically from the right plot in the second row, we can see that for deep levels of MLMC, the kurtosis increases dramatically with respect to level ℓ of the MLMC method. This poor behavior of the kurtosis is mainly due to the *catastrophic coupling* issue (explained in Section 1.4.1), as illustrated by Figures 5.3, 5.5 and 5.7.

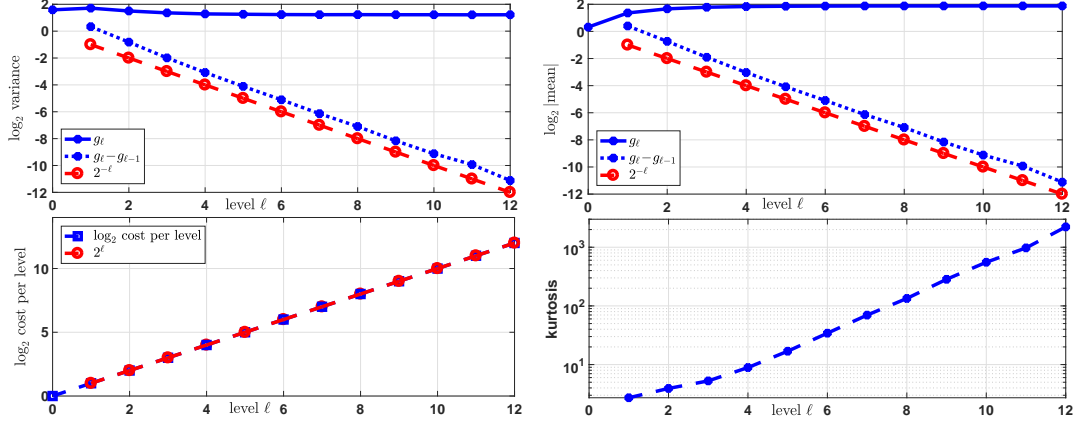


Figure 5.2: MLMC without IS for Example 5.1: Convergence plots with $g_\ell = \overline{X}_\ell(T)$.

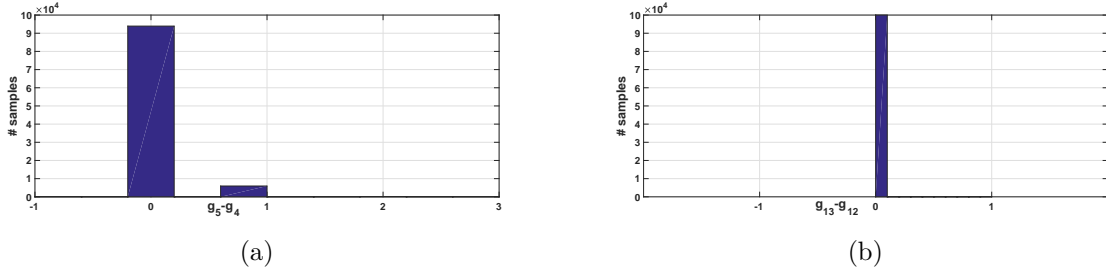


Figure 5.3: Example 5.1 without IS: Histogram of $g_\ell - g_{\ell-1}$ ($g_\ell = \overline{X}_\ell(T)$), for number of samples $M_\ell = 10^5$. The proportion of samples $\{g_\ell - g_{\ell-1} = 0\}$ is an increasing function of the level, ℓ , of the MLMC estimator, to reach almost 100% for $\ell = 13$. a) $\ell = 5$. b) $\ell = 13$.

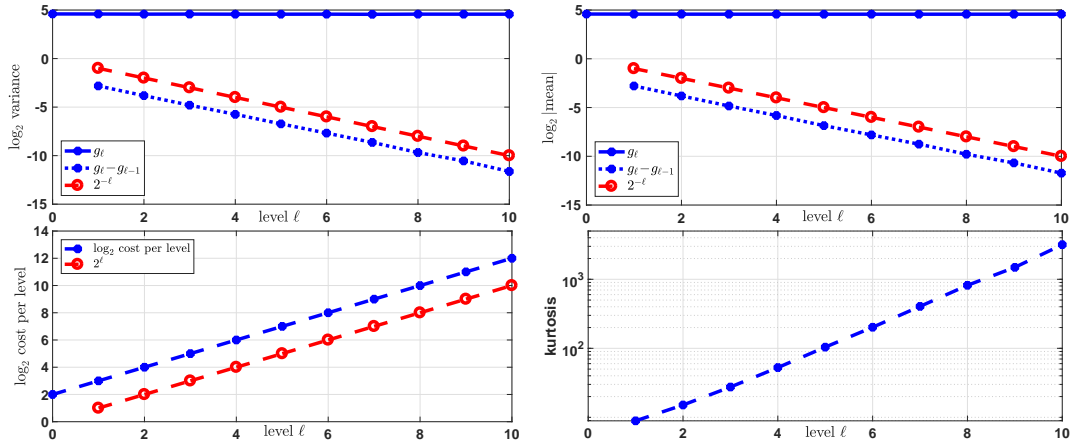


Figure 5.4: Convergence plots of MLMC without IS for Example 5.2.

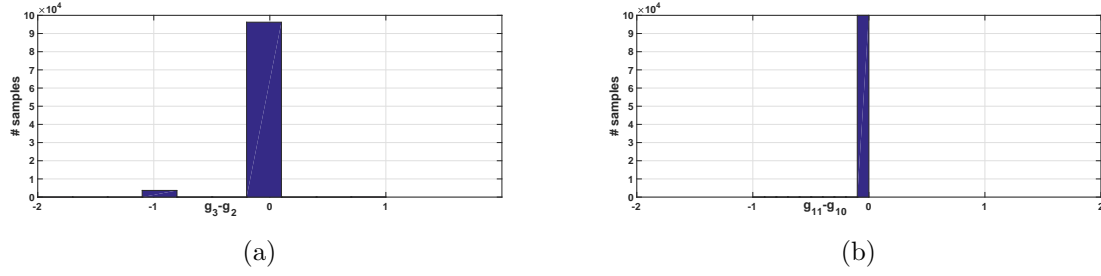


Figure 5.5: Example 5.2 without IS: Histogram of $g_\ell - g_{\ell-1}$ ($g_\ell = \overline{X}_\ell^{(1)}(T)$), for number of samples $M_\ell = 10^5$. The proportion of samples $\{g_\ell - g_{\ell-1} = 0\}$ is an increasing function of the level, ℓ , of the MLMC estimator, to reach almost 100% for $\ell = 11$. a) $\ell = 3$. b) $\ell = 11$.

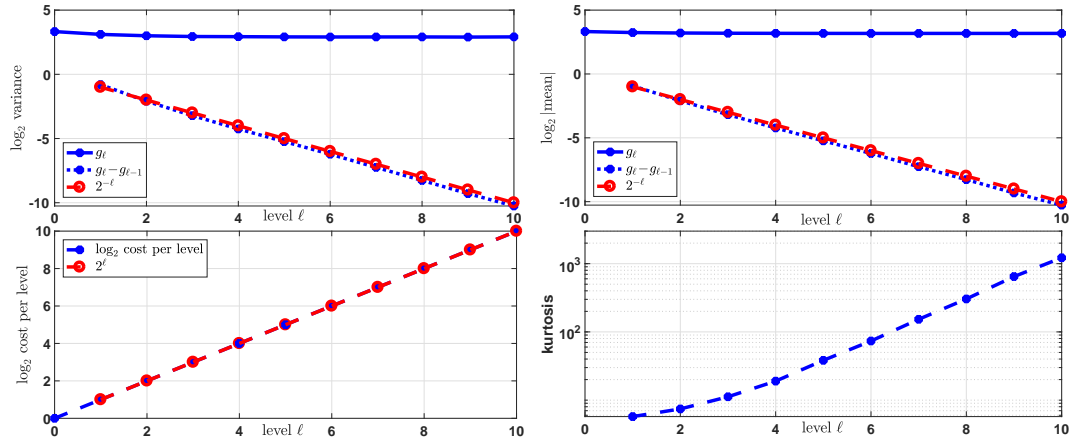


Figure 5.6: Convergence plots of MLMC without IS for Example 5.3.

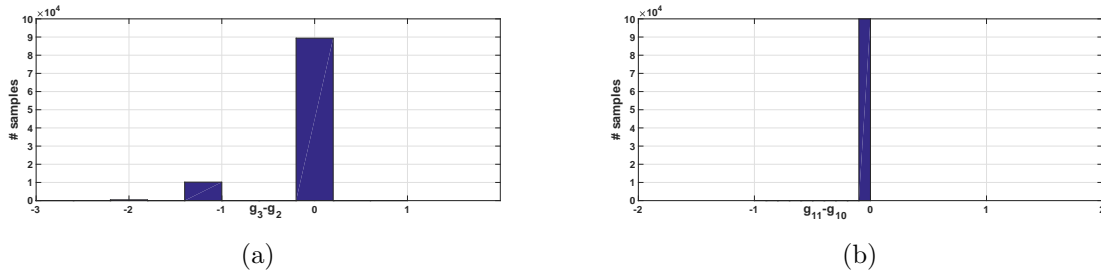


Figure 5.7: Example 5.3 without IS: Histogram of $g_\ell - g_{\ell-1}$ ($g_\ell = \overline{X}_\ell^{(3)}(T)$), for number of samples $M_\ell = 10^5$. The proportion of samples $\{g_\ell - g_{\ell-1} = 0\}$ is an increasing function of the level, ℓ , of the MLMC estimator, to reach almost 100% for $\ell = 11$. a) $\ell = 3$. b) $\ell = 11$.

5.2 Numerical Results of MLMC With IS

The MLMC estimator in combination with IS reduces the kurtosis significantly and improves the strong convergence rate from 1 to $1 + \delta$, as illustrated by Figures 5.9, and 5.10 for Example 5.1, Figures 5.12, 5.13 for Example 5.2, and Figures 5.15, and 5.16 for Example 5.3. The notable reduction of the kurtosis is mainly due to the small reduction of the proportion of identical terminal values, g_ℓ and $g_{\ell-1}$, after using IS, as can be seen in Figures 5.8, 5.11 and 5.14.

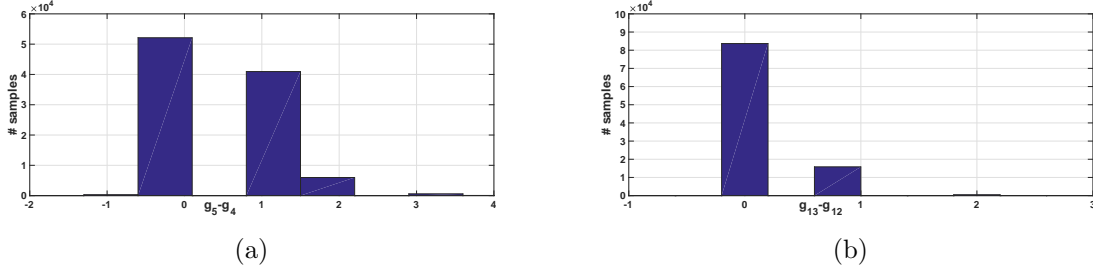


Figure 5.8: Example 5.1 with IS ($\delta = \frac{3}{4}$): Histogram of $g_\ell - g_{\ell-1}$ ($g_\ell = \bar{X}_\ell(T)$), for number of samples $M_\ell = 10^5$. Our IS reduces the the proportion of samples $\{g_\ell - g_{\ell-1} = 0\}$ (compared to the case without IS; see Figure 5.3) to reach around 80% for $\ell = 13$. a) $\ell = 5$. b) $\ell = 13$.

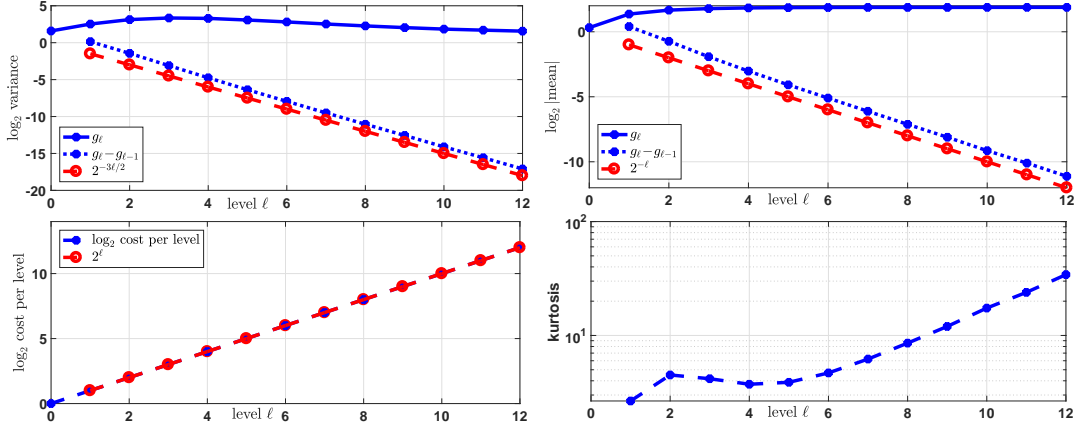


Figure 5.9: Convergence plots of MLMC with IS ($\delta = 1/2$) for Example 5.1.

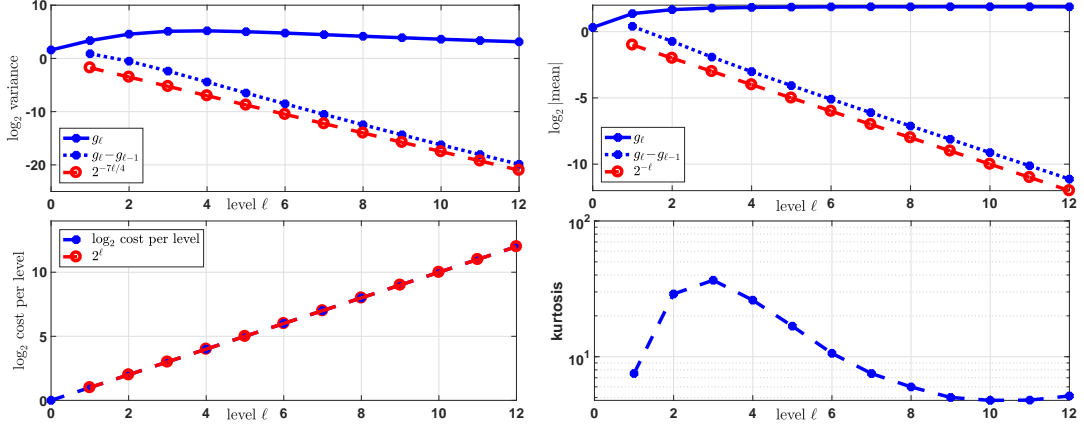


Figure 5.10: Convergence plots of MLMC with IS ($\delta = 3/4$) for Example 5.1.

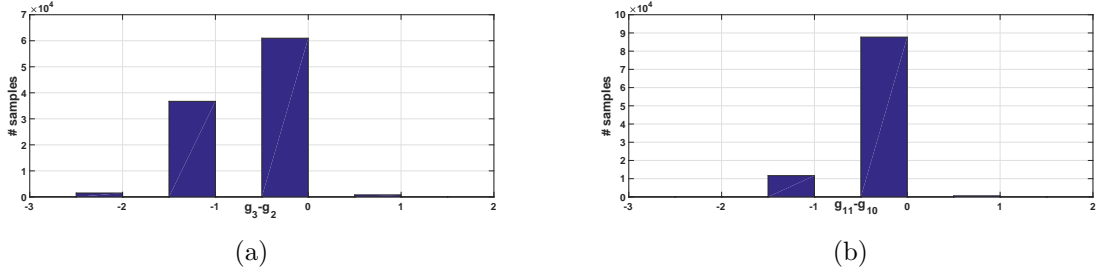


Figure 5.11: Example 5.2 with IS ($\delta = \frac{3}{4}$): Histogram of $g_\ell - g_{\ell-1}$ ($g_\ell = \overline{X}_\ell^{(1)}(T)$), for number of samples $M_\ell = 10^5$. Our IS reduces the the proportion of samples $\{g_\ell - g_{\ell-1} = 0\}$ (compared to the case without IS; see Figure 5.5) to reach around 90% for $\ell = 11$. a) $\ell = 3$. b) $\ell = 11$.

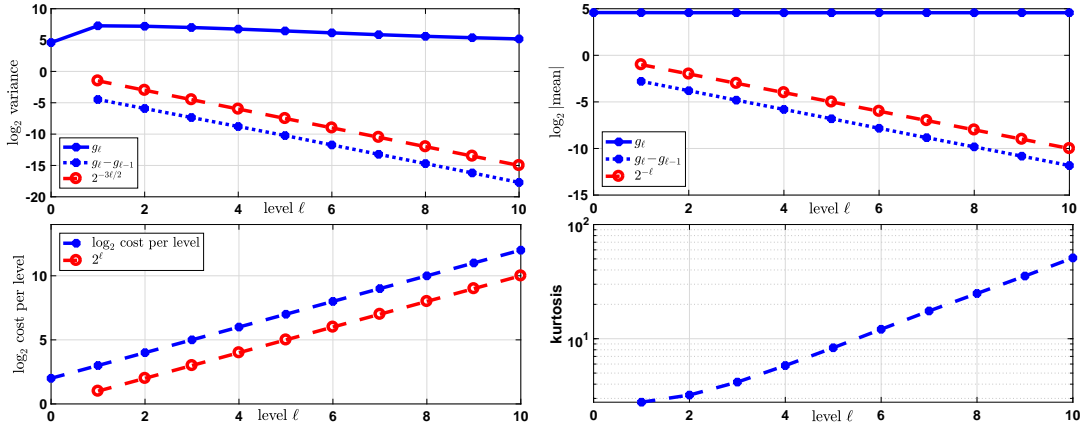


Figure 5.12: Convergence plots of MLMC with IS ($\delta = 1/2$) for Example 5.2.

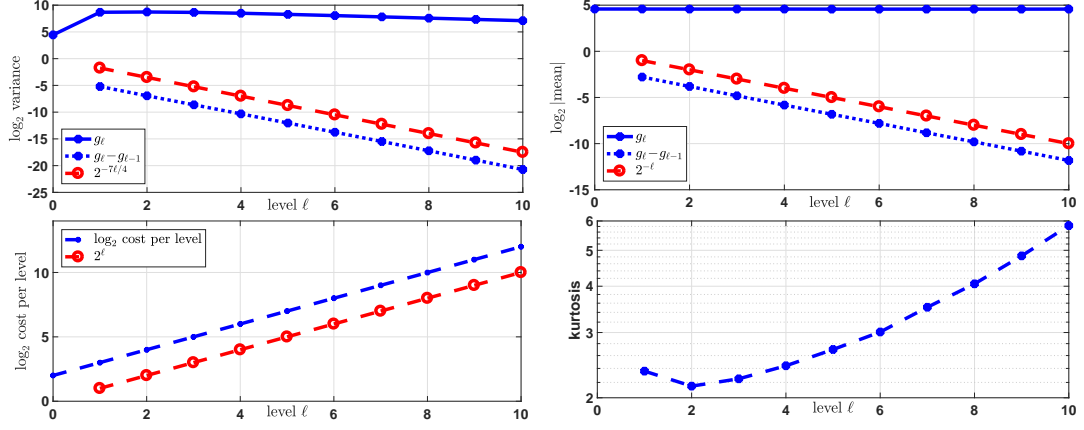


Figure 5.13: Convergence plots of MLMC with IS ($\delta = 3/4$) for Example 5.2.

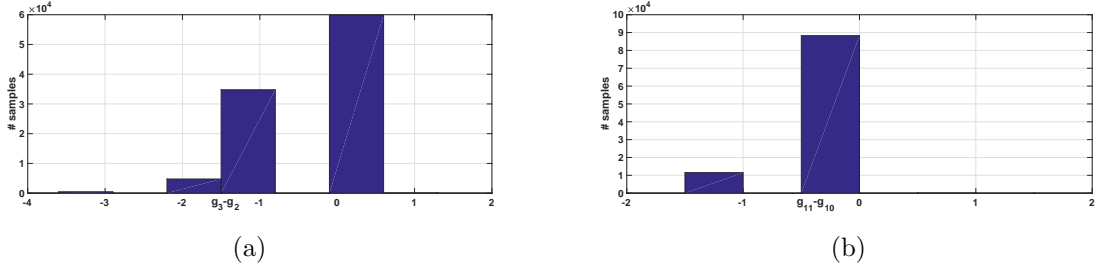


Figure 5.14: Example 5.3 with IS ($\delta = \frac{3}{4}$): Histogram of $g_\ell - g_{\ell-1}$ ($g_\ell = \overline{X}_\ell^{(3)}(T)$), for number of samples $M_\ell = 10^5$. Our IS reduces the the proportion of samples $\{g_\ell - g_{\ell-1} = 0\}$ (compared to the case without IS; see Figure 5.7) to reach around 90% for $\ell = 11$. a) $\ell = 3$. b) $\ell = 11$.

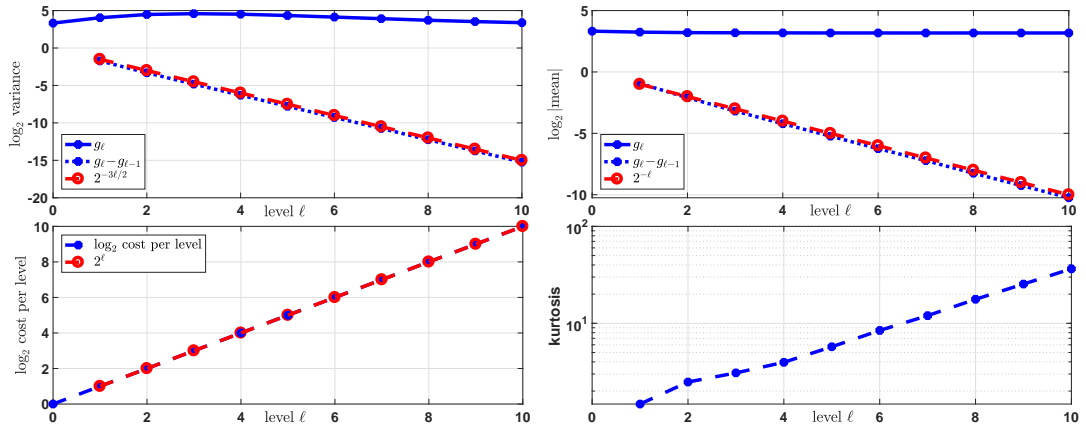


Figure 5.15: Convergence plots of MLMC with IS ($\delta = 1/2$) for Example 5.3.

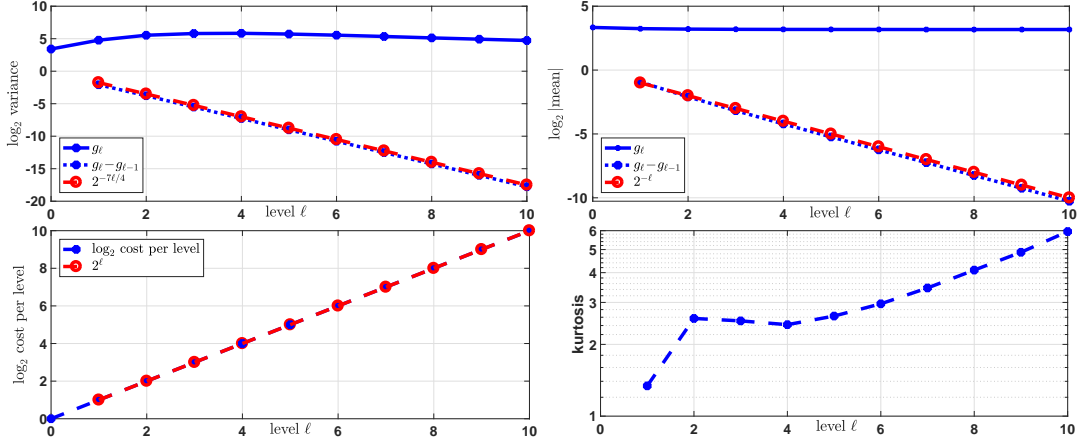


Figure 5.16: Convergence plots of MLMC with IS ($\delta = 3/4$) for Example 5.3.

6 Conclusions and Future Work

In the work presented here, we address the high-kurtosis phenomenon related to catastrophic coupling, and observed in MLMC estimators when applied in the context of SRNs and pure jumps. We propose a novel path-dependent IS algorithm to be used with MLMC, in order to improve robustness and computational performance.

Our theoretical results and numerical experiments show that our proposed method not only improves the robustness of the multilevel estimator by dramatically reducing the kurtosis, but also improves the strong convergence rate, which results in an improvement of the complexity of the MLMC method, from $\mathcal{O}(\text{TOL}^{-2} \log(\text{TOL})^2)$ to $\mathcal{O}(\text{TOL}^{-2})$, with TOL being a pre-selected tolerance. We achieve all these improvements with a negligible additional cost since our IS algorithm is only applied a few times across each simulated path.

Here, we limit ourselves to the use of the IS technique with an explicit TL scheme. In a future study, we intend to investigate the potential of our proposed algorithm when using a split-step implicit TL scheme, as proposed in [27], which is required for systems with the presence of slow and fast timescales (stiff systems). To overcome the *catastrophic coupling* issue, the authors in [27] used extrapolation to estimate the sample variance when using MLMC. We believe that our new IS technique may help to obtain accurate estimates of the sample variances needed by the MLMC estimator. Another potential research direction may be to investigate a more optimal IS scheme to be used for MLMC; for instance, we may try to use a hierarchy of δ_ℓ , where the parameter δ used in our proposed method would depend on the level of discretization. Furthermore, we may explore the possibility of introducing a new IS scheme for MLMC based on SPM coupling, to address the *catastrophic decoupling* issue, which is the second cause of the high-kurtosis phenomenon in the context of SRNs when using MLMC. Finally, we can combine the strengths of our method and the hybrid approach in [36] to improve the performance of the MLMC estimator.

Acknowledgments This work was supported by the KAUST Office of Sponsored Research (OSR) under Award No. URF/1/2584-01-01 and the Alexander von Humboldt Foundation. C. Ben Hammouda and R. Tempone are members of the KAUST SRI Center for Uncertainty Quantification in Computational Science and Engineering. The authors would like to thank Dr. Alvaro Moraes

and Sophia Franziska Wiechert for their helpful and constructive comments. The authors are also very grateful to the anonymous referees for their valuable comments and suggestions that greatly contributed to shape the final version of the work.

References Cited

- [1] Assyr Abdulle, Yucheng Hu, and Tiejun Li. Chebyshev methods with discrete noise: the τ -rock methods. *Journal of Computational Mathematics*, pages 195–217, 2010.
- [2] Tae-Hyuk Ahn, Adrian Sandu, and Xiaoying Han. Implicit simulation methods for stochastic chemical kinetics. *arXiv preprint arXiv:1303.3614*, 2013.
- [3] D. Anderson and D. Higham. Multilevel Monte Carlo for continuous Markov chains, with applications in biochemical kinetics. *SIAM Multiscale Model. Simul.*, 10(1), 2012.
- [4] David F Anderson. A modified next reaction method for simulating chemical systems with time dependent propensities and delays. *The Journal of chemical physics*, 127(21):214107, 2007.
- [5] David F Anderson, Arnab Ganguly, Thomas G Kurtz, et al. Error analysis of tau-leap simulation methods. *The Annals of Applied Probability*, 21(6):2226–2262, 2011.
- [6] David F Anderson, Desmond J Higham, and Yu Sun. Multilevel Monte Carlo for stochastic differential equations with small noise. *SIAM Journal on Numerical Analysis*, 54(2):505–529, 2016.
- [7] David F Anderson and Thomas G Kurtz. *Stochastic analysis of biochemical systems*, volume 1. Springer, 2015.
- [8] Juan P Aparicio and Hernán G Solari. Population dynamics: Poisson approximation and its relation to the langevin process. *Physical Review Letters*, 86(18):4183, 2001.
- [9] Christian Bayer, Chiheb Ben Hammouda, and Raul Tempone. Numerical smoothing and hierarchical approximations for efficient option pricing and density estimation. *arXiv preprint arXiv:2003.05708*, 2020.
- [10] Alexandros Beskos, Ajay Jasra, Kody Law, Raul Tempone, and Yan Zhou. Multilevel sequential Monte Carlo samplers. *Stochastic Processes and their Applications*, 127(5):1417–1440, 2017.
- [11] Fred Brauer and Carlos Castillo-Chavez. *Mathematical models in population biology and epidemiology*, volume 40. Springer.
- [12] Yang Cao and Linda Petzold. Trapezoidal tau-leaping formula for the stochastic simulation of biochemical systems. *Proceedings of Foundations of Systems Biology in Engineering (FOSBE 2005)*, pages 149–152, 2005.
- [13] Youfang Cao and Jie Liang. Adaptively biased sequential importance sampling for rare events in reaction networks with comparison to exact solutions from finite buffer dCME method. *The Journal of chemical physics*, 139(2):07B605_1, 2013.

- [14] Erhan Çinlar. *Probability and stochastics*, volume 261. Springer Science & Business Media, 2011.
- [15] K Andrew Cliffe, Mike B Giles, Robert Scheichl, and Aretha L Teckentrup. Multilevel Monte Carlo methods and applications to elliptic PDEs with random coefficients. *Computing and Visualization in Science*, 14(1):3, 2011.
- [16] Bernie J Daigle Jr, Min K Roh, Dan T Gillespie, and Linda R Petzold. Automated estimation of rare event probabilities in biochemical systems. *The Journal of chemical physics*, 134(4):01B628, 2011.
- [17] Darrell Duffie, Peter Glynn, et al. Efficient Monte Carlo simulation of security prices. *The Annals of Applied Probability*, 5(4):897–905, 1995.
- [18] Stefan Engblom. On the stability of stochastic jump kinetics. *arXiv preprint arXiv:1202.3892*, 2012.
- [19] Stewart N. Ethier and Thomas G. Kurtz. *Markov processes : characterization and convergence*. Wiley series in probability and mathematical statistics. J. Wiley & Sons, New York, Chichester, 1986.
- [20] Michael B Giles. Multilevel Monte Carlo path simulation. *Operations Research*, 56(3):607–617, 2008.
- [21] Michael B Giles. Multilevel Monte Carlo methods. *Acta Numerica*, 24:259–328, 2015.
- [22] Daniel T Gillespie. A general method for numerically simulating the stochastic time evolution of coupled chemical reactions. *Journal of computational physics*, 22(4):403–434, 1976.
- [23] Daniel T Gillespie. The chemical Langevin equation. *The Journal of Chemical Physics*, 113(1):297–306, 2000.
- [24] Daniel T Gillespie. Approximate accelerated stochastic simulation of chemically reacting systems. *The Journal of Chemical Physics*, 115(4):1716–1733, 2001.
- [25] Wenhui Gou. Estimating value-at-risk using multilevel Monte Carlo maximum entropy method, 2016.
- [26] Ankit Gupta, Corentin Briat, and Mustafa Khammash. A scalable computational framework for establishing long-term behavior of stochastic reaction networks. *PLoS computational biology*, 10(6):e1003669, 2014.
- [27] Chiheb Ben Hammouda, Alvaro Moraes, and Raúl Tempone. Multilevel hybrid split-step implicit tau-leap. *Numerical Algorithms*, 74(2):527–560, 2017.
- [28] Sebastian C Hensel, James B Rawlings, and John Yin. Stochastic kinetic modeling of vesicular stomatitis virus intracellular growth. *Bulletin of mathematical biology*, 71(7):1671–1692, 2009.
- [29] Ahmed Kebaier et al. Statistical Romberg extrapolation: a new variance reduction method and applications to option pricing. *The Annals of Applied Probability*, 15(4):2681–2705, 2005.

- [30] Hiroyuki Kuwahara and Ivan Mura. An efficient and exact stochastic simulation method to analyze rare events in biochemical systems. *The Journal of chemical physics*, 129(16):10B619, 2008.
- [31] Christopher Lester, Ruth E Baker, Michael B Giles, and Christian A Yates. Extending the multi-level method for the simulation of stochastic biological systems. *Bulletin of mathematical biology*, 78(8):1640–1677, 2016.
- [32] Christopher Lester, Christian A Yates, and Ruth E Baker. Robustly simulating biochemical reaction kinetics using multi-level Monte Carlo approaches. *Journal of Computational Physics*, 375:1401–1423, 2018.
- [33] Christopher Lester, Christian Adam Yates, Michael B Giles, and Ruth E Baker. An adaptive multi-level simulation algorithm for stochastic biological systems. *The Journal of chemical physics*, 142(2):01B612.1, 2015.
- [34] Tiejun Li. Analysis of explicit tau-leaping schemes for simulating chemically reacting systems. *Multiscale Modeling & Simulation*, 6(2):417–436, 2007.
- [35] Alvaro Moraes, Raúl Tempone, and Pedro Vilanova. A multilevel adaptive reaction-splitting simulation method for stochastic reaction networks. *SIAM Journal on Scientific Computing*, 38(4):A2091–A2117, 2016.
- [36] Alvaro Moraes, Raul Tempone, and Pedro Vilanova. Multilevel hybrid Chernoff tau-leap. *BIT Numerical Mathematics*, 56(1):189–239, 2016.
- [37] Christopher V Rao and Adam P Arkin. Stochastic chemical kinetics and the quasi-steady-state assumption: Application to the Gillespie algorithm. *The Journal of chemical physics*, 118(11):4999–5010, 2003.
- [38] Muruhan Rathinam. Moment growth bounds on continuous time Markov processes on non-negative integer lattices. *arXiv preprint arXiv:1304.5169*, 2013.
- [39] Muruhan Rathinam and Hana El Samad. Reversible-equivalent-monomolecular tau: A leaping method for small number and stiff stochastic chemical systems. *Journal of Computational Physics*, 224(2):897–923, 2007.
- [40] Ranjan Srivastava, L You, J Summers, and J Yin. Stochastic vs. deterministic modeling of intracellular viral kinetics. *Journal of theoretical biology*, 218(3):309–321, 2002.
- [41] David J Warne, Ruth E Baker, and Matthew J Simpson. Multilevel rejection sampling for approximate Bayesian computation. *Computational Statistics & Data Analysis*, 124:71–86, 2018.
- [42] David J Warne, Ruth E Baker, and Matthew J Simpson. Simulation and inference algorithms for stochastic biochemical reaction networks: from basic concepts to state-of-the-art. *Journal of the Royal Society Interface*, 16(151):20180943, 2019.

A Proofs of Lemma 4.1 and Theorems 4.1 and 4.2

Proof of Lemma 4.1. We denote by $K = \sum_{n \in S} k_n$, $L_\ell(j)$ the likelihood evaluated at $K = j$. Then, for $p \geq 1$ and $0 \leq \delta < 1$, and using relation (4.4), we write

$$\begin{aligned}
 \mathbb{E}_{\bar{\pi}_\ell} [|\Delta g_\ell|^p(T) L_\ell^p; (\mathcal{F}_{N_\ell-1}, \mathcal{I}_\ell^s = \mathcal{S})] &= \sum_{\substack{|\Delta g_\ell(T)|=K=i \\ i \in \mathbb{N} \setminus \{0\}}} i^p L_\ell^p(i) \bar{\pi}_\ell(|\Delta g_\ell(T)| = i, K = i; (\mathcal{F}_{N_\ell-1}, \mathcal{I}_\ell^s = \mathcal{S})) \\
 &+ \sum_{\substack{|\Delta g_\ell(T)|=i, K=j \\ i \neq j, (i,j) \in \mathbb{N}^2}} i^p L_\ell^p(j) \bar{\pi}_\ell(|\Delta g_\ell(T)| = i, K = j; (\mathcal{F}_{N_\ell-1}, \mathcal{I}_\ell^s = \mathcal{S})) \\
 &= \sum_{\substack{|\Delta g_\ell(T)|=K=i \\ i \in \mathbb{N} \setminus \{0\}}} \underbrace{i^p e^{p(\Delta t_\ell^{1-\delta} - \Delta t_\ell) \sum_{n \in S} \Delta a_{\ell,n}} \Delta t_\ell^{ip\delta} \bar{\pi}_\ell(|\Delta g_\ell(T)| = i, K = i; (\mathcal{F}_{N_\ell-1}, \mathcal{I}_\ell^s = \mathcal{S}))}_{A_i} \\
 &+ \sum_{\substack{|\Delta g_\ell(T)|=i \\ K=j \\ i \neq j, (i,j) \in \mathbb{N}^2}} \underbrace{i^p e^{p(\Delta t_\ell^{1-\delta} - \Delta t_\ell) \sum_{n \in S} \Delta a_{\ell,n}} \Delta t_\ell^{jp\delta} \bar{\pi}_\ell(|\Delta g_\ell(T)| = i, K = j; (\mathcal{F}_{N_\ell-1}, \mathcal{I}_\ell^s = \mathcal{S}))}_{B_{ij}} \\
 (A.1) \quad &= \sum_{\substack{|\Delta g_\ell(T)|=K=i \\ i \in \mathbb{N} \setminus \{0\}}} A_i + \sum_{\substack{|\Delta g_\ell(T)|=i, K=j \\ i \neq j, (i,j) \in \mathbb{N}^2}} B_{ij}.
 \end{aligned}$$

Using Assumption 4.1 (a), we have

$$(A.2) \quad 0 \leq \frac{\sum_{\substack{|\Delta g_\ell(T)|=K=i \\ i \in \mathbb{N} \setminus \{0,1\}}} A_i}{A_1} \leq \underbrace{\sum_{i \in \mathbb{N} \setminus \{0,1\}} i^p \Delta t_\ell^{(i-1)p\delta}}_{\xrightarrow[\Delta t_\ell \rightarrow 0]{0}}.$$

Now, let us examine the second sum in the right-hand side of (A.1). First, observe that $B_{0j} = 0, \forall j \geq 1$ and $B_{i0} = 0, \forall i \geq 1$. Although the first observation is clear, we need to explain the second observation, which is mainly due to the fact that $\bar{\pi}(|\Delta g_\ell(T)| = i, K = 0; (\mathcal{F}_{N_\ell-1}, \mathcal{I}_\ell^s = \mathcal{S})) = 0, \forall i \geq 1$. For the purpose of simplification, let us consider $g_\ell = \bar{X}_\ell$; then considering the first interval in the coarse level, and using the coupling equation (2.6), we have: i) At $t = 0$: $\bar{X}_\ell(0) = \bar{X}_{\ell-1}(0)$ and $\Delta a_{\ell-1,0}^1 = 0$. ii) At $t = \Delta t_\ell$: $\bar{X}_\ell(\Delta t_\ell) = \bar{X}_{\ell-1}(\Delta t_\ell)$ and $\Delta a_{\ell-1,0}^2 = a(\bar{X}_\ell(\Delta t_\ell)) - a(\bar{X}_{\ell-1}(0))$. iii) At $t = t_1 = 2\Delta t_\ell$: if $\Delta a_{\ell-1,0}^2 = 0$, then we simulate this step under the old measure and consequently we will have $\bar{X}_\ell(t_1) = \bar{X}_{\ell-1}(t_1)$ otherwise if $\Delta a_{\ell-1,0}^2 \neq 0$, then we simulate this step under the IS measure, but since $j = 0$, then we will have $\bar{X}_\ell(t_1) = \bar{X}_{\ell-1}(t_1)$. Therefore, in both scenarios, we will have the same situation at the start, $t_0 = 0$. Therefore, we conclude that $\bar{\pi}(|\Delta g_\ell(T)| = i, K = 0; (\mathcal{F}_{N_\ell-1}, \mathcal{I}_\ell^s = \mathcal{S})) = 0, \forall i \geq 1$ and $B_{i0} = 0, \forall i \geq 1$.

Then, using Assumptions 4.1 (b) and 4.1 (c), we obtain

$$\begin{aligned}
0 &\leq \frac{\sum_{\substack{|\Delta g_\ell(T)|=i, K=j \\ i \neq j, (i,j) \in \mathbb{N}^2}} B_{ij}}{A_1} \leq \frac{\sum_{i \neq j, 1 \leq i,j} i^p \Delta t_\ell^{jp\delta} \bar{\pi}_\ell \{|\Delta g_\ell(T)| = i; (\mathcal{F}_{N_\ell-1}, \mathcal{I}_\ell^s = \mathcal{S})\}}{(\Delta t_\ell^{p\delta}) e^{-(\Delta t_\ell^{1-\delta} \Delta a_{\ell,n^*})} (\Delta t_\ell^{1-\delta} \Delta a_{\ell,n^*}) (1 + o(1))} \\
&\leq \frac{\sum_{i \neq j, 1 \leq i,j} \eta_{i,\ell} i^p \Delta t_\ell^{jp\delta} \Delta t_\ell^{i(1-\delta)}}{(\Delta t_\ell^{p\delta}) e^{-(\Delta t_\ell^{1-\delta} \Delta a_{\ell,n^*})} (\Delta t_\ell^{1-\delta} \Delta a_{\ell,n^*}) (1 + o(1))} \\
(A.3) \quad &= \underbrace{(1 + o(1))^{-1} \left(e^{(\Delta t_\ell^{1-\delta} \Delta a_{\ell,n^*})} \Delta a_{\ell,n^*}^{-1} \sum_{i \neq j, 1 \leq i,j} \eta_{i,\ell} i^p \Delta t_\ell^{jp\delta(j-1)} \Delta t_\ell^{(1-\delta)(i-1)} \right)}_{\xrightarrow[\Delta t_\ell \rightarrow 0]{0}}.
\end{aligned}$$

Therefore, using (A.1), (A.2) and (A.3), we conclude Lemma 4.1, that is

$$\begin{aligned}
\mathbb{E}_{\bar{\pi}_\ell} [|\Delta g_\ell|^p(T) L_\ell^p; (\mathcal{F}_{N_\ell-1}, \mathcal{I}_\ell^s = \mathcal{S})] &= \Delta t_\ell^{(p-1)\delta+1} (\Delta a_{\ell,n^*}) e^{p(\Delta t_\ell^{1-\delta} - \Delta t_\ell) \sum_{n \in \mathcal{S}} \Delta a_{\ell,n}} e^{-(\Delta t_\ell^{1-\delta} \Delta a_{\ell,n^*})} (1 + h_{p,\ell}), \\
\text{such that } h_{p,\ell} &\xrightarrow[\Delta t_\ell \rightarrow 0]{} 0. \quad \square
\end{aligned}$$

Proof of Theorem 4.1. Let $0 \leq \delta < 1$. In the first step of the proof, we want to show that

$$\kappa_\ell := \frac{\mathbb{E}_{\bar{\pi}_\ell} [(Y_\ell - \mathbb{E}_{\bar{\pi}_\ell} [Y_\ell])^4]}{(\text{Var}_{\bar{\pi}_\ell} [Y_\ell])^2} \underset{\Delta t_\ell \rightarrow 0}{\sim} \frac{\mathbb{E}_{\bar{\pi}_\ell} [Y_\ell^4]}{(\mathbb{E}_{\bar{\pi}_\ell} [Y_\ell^2])^2}$$

Let us first show that $\text{Var}_{\bar{\pi}_\ell} [Y_\ell] \underset{\Delta t_\ell \rightarrow 0}{\sim} \mathbb{E}_{\bar{\pi}_\ell} [Y_\ell^2]$. In fact,

$$\frac{\text{Var}_{\bar{\pi}_\ell} [Y_\ell]}{\mathbb{E}_{\bar{\pi}_\ell} [Y_\ell^2]} = \frac{\mathbb{E}_{\bar{\pi}_\ell} [Y_\ell^2] - (\mathbb{E}_{\bar{\pi}_\ell} [Y_\ell])^2}{\mathbb{E}_{\bar{\pi}_\ell} [Y_\ell^2]} = 1 - \frac{(\mathbb{E}_{\bar{\pi}_\ell} [Y_\ell])^2}{\mathbb{E}_{\bar{\pi}_\ell} [Y_\ell^2]}.$$

Therefore, we need to show that $I_1 := \frac{(\mathbb{E}_{\bar{\pi}_\ell} [Y_\ell])^2}{\mathbb{E}_{\bar{\pi}_\ell} [Y_\ell^2]} \xrightarrow[\Delta t_\ell \rightarrow 0]{} 0$.

Due to the order one weak error convergence, there exists a constant $d_1 > 0$ such that $(\mathbb{E}_{\bar{\pi}_\ell} [Y_\ell]) \leq d_1 \Delta t_\ell$. Therefore, using Lemma 4.1 and Assumption 4.2, we obtain

$$\begin{aligned}
0 \leq I_1 &\leq \frac{d_1^2 \Delta t_\ell^2}{\mathbb{E}_{\bar{\pi}_\ell} [Y_\ell^2]} = \frac{d_1^2 \Delta t_\ell^2}{\mathbb{E}_{\bar{\pi}_\ell} [\mathbb{E}_{\bar{\pi}_\ell} [Y_\ell^2; (\mathcal{F}_{N_\ell}, \mathcal{I}_\ell^s = \mathcal{S})]]} \\
&= \frac{d_1^2 \Delta t_\ell^2}{\mathbb{E}_{\bar{\pi}_\ell} \left[(\Delta t_\ell^{\delta+1}) e^{2(\Delta t_\ell^{1-\delta} - \Delta t_\ell) \sum_{n \in \mathcal{S}} \Delta a_{\ell,n}} e^{-(\Delta t_\ell^{1-\delta} \Delta a_{\ell,n^*})} (\Delta a_{\ell,n^*}) (1 + h_{2,\ell}) \right]} \\
&\leq \frac{d_1^2 \Delta t_\ell^{1-\delta}}{\mathbb{E}_{\bar{\pi}_\ell} \left[e^{-(\Delta t_\ell^{1-\delta} \Delta a_{\ell,n^*})} \Delta a_{\ell,n^*} \right]} \leq \frac{d_1^2 \Delta t_\ell^{1-\delta}}{C_1} \xrightarrow[\Delta t_\ell \rightarrow 0]{} 0.
\end{aligned}$$

Therefore, we conclude that

$$(A.4) \quad \text{Var}_{\bar{\pi}_\ell} [Y_\ell] \underset{\Delta t_\ell \rightarrow 0}{\sim} \mathbb{E}_{\bar{\pi}_\ell} [Y_\ell^2].$$

Now, let us show that $\mathbb{E}_{\pi_\ell} \left[(Y_\ell - \mathbb{E}_{\pi_\ell} [Y_\ell])^4 \right] \underset{\Delta t_\ell \rightarrow 0}{\sim} \mathbb{E}_{\pi_\ell} [Y_\ell^4]$. In fact,

$$\begin{aligned} \frac{\mathbb{E}_{\pi_\ell} \left[(Y_\ell - \mathbb{E}_{\pi_\ell} [Y_\ell])^4 \right]}{\mathbb{E}_{\pi_\ell} [Y_\ell^4]} &= \frac{\mathbb{E}_{\pi_\ell} [Y_\ell^4] - 4\mathbb{E}_{\pi_\ell} [Y_\ell^3] \mathbb{E}_{\pi_\ell} [Y_\ell] + 6\mathbb{E}_{\pi_\ell} [Y_\ell^2] (\mathbb{E}_{\pi_\ell} [Y_\ell])^2 - 3(\mathbb{E}_{\pi_\ell} [Y_\ell])^4}{\mathbb{E}_{\pi_\ell} [Y_\ell^4]} \\ &= 1 - 4 \frac{\mathbb{E}_{\pi_\ell} [Y_\ell^3] \mathbb{E}_{\pi_\ell} [Y_\ell]}{\mathbb{E}_{\pi_\ell} [Y_\ell^4]} + 6 \frac{\mathbb{E}_{\pi_\ell} [Y_\ell^2] (\mathbb{E}_{\pi_\ell} [Y_\ell])^2}{\mathbb{E}_{\pi_\ell} [Y_\ell^4]} - 3 \frac{(\mathbb{E}_{\pi_\ell} [Y_\ell])^4}{\mathbb{E}_{\pi_\ell} [Y_\ell^4]} \\ &= 1 - 4I_2 + 6I_3 - 3I_4 \end{aligned}$$

Therefore, we need to show that $I_2, I_3, I_4 \xrightarrow{\Delta t_\ell \rightarrow 0} 0$.

Using Lemma 4.1 and Assumption 4.2, we obtain

$$\begin{aligned} 0 \leq I_4 &\leq \frac{d_1^4 \Delta t_\ell^4}{\mathbb{E}_{\pi_\ell} [Y_\ell^4]} = \frac{d_1^4 \Delta t_\ell^4}{\mathbb{E}_{\pi_\ell} [\mathbb{E}_{\pi_\ell} [Y_\ell^4; (\mathcal{F}_{N_\ell}, \mathcal{I}_\ell^s = \mathcal{S})]]} \\ &= \frac{d_1^4 \Delta t_\ell^4}{\mathbb{E}_{\pi_\ell} \left[\left((\Delta t_\ell^{3\delta+1}) e^{4(\Delta t_\ell^{1-\delta} - \Delta t_\ell) \sum_{n \in \mathcal{S}} \Delta a_{\ell,n}} e^{-(\Delta t_\ell^{1-\delta} \Delta a_{\ell,n^*})} (\Delta a_{\ell,n^*}) (1 + h_{4,\ell}) \right) \right]} \\ &\leq \frac{d_1^4 \Delta t_\ell^{3(1-\delta)}}{\mathbb{E}_{\pi_\ell} \left[e^{-(\Delta t_\ell^{1-\delta} \Delta a_{\ell,n^*})} \Delta a_{\ell,n^*} \right]} \leq \frac{d_1^4 \Delta t_\ell^{3(1-\delta)}}{C_1} \xrightarrow{\Delta t_\ell \rightarrow 0} 0. \end{aligned}$$

Similarly for I_2 , using Lemma 4.1 and Assumptions 4.2 and 4.3, we obtain

$$\begin{aligned} 0 \leq I_2 &\leq \frac{d_1 \Delta t_\ell \mathbb{E}_{\pi_\ell} [|Y_\ell|^3]}{\mathbb{E}_{\pi_\ell} [Y_\ell^4]} = \frac{d_1 \Delta t_\ell \mathbb{E}_{\pi_\ell} [\mathbb{E}_{\pi_\ell} [Y_\ell^3; (\mathcal{F}_{N_\ell}, \mathcal{I}_\ell^s = \mathcal{S})]]}{\mathbb{E}_{\pi_\ell} [\mathbb{E}_{\pi_\ell} [Y_\ell^4; (\mathcal{F}_{N_\ell}, \mathcal{I}_\ell^s = \mathcal{S})]]} \\ &= \frac{d_1 \Delta t_\ell \mathbb{E}_{\pi_\ell} \left[\left((\Delta t_\ell^{2\delta+1}) e^{3(\Delta t_\ell^{1-\delta} - \Delta t_\ell) \sum_{n \in \mathcal{S}} \Delta a_{\ell,n}} e^{-(\Delta t_\ell^{1-\delta} \Delta a_{\ell,n^*})} (\Delta a_{\ell,n^*}) (1 + h_{3,\ell}) \right) \right]}{\mathbb{E}_{\pi_\ell} \left[\left((\Delta t_\ell^{3\delta+1}) e^{4(\Delta t_\ell^{1-\delta} - \Delta t_\ell) \sum_{n \in \mathcal{S}} \Delta a_{\ell,n}} e^{-(\Delta a_{\ell,n^*})} (\Delta t_\ell^{1-\delta} \Delta a_{\ell,n^*}) (1 + h_{4,\ell}) \right) \right]} \\ &\leq \frac{d_1 \Delta t_\ell^{1-\delta} \mathbb{E}_{\pi_\ell} \left[e^{3(\Delta t_\ell^{1-\delta} - \Delta t_\ell) \sum_{n \in \mathcal{S}} \Delta a_{\ell,n}} \Delta a_{\ell,n^*} (1 + h_{3,\ell}) \right]}{\mathbb{E}_{\pi_\ell} \left[e^{-(\Delta t_\ell^{1-\delta} \Delta a_{\ell,n^*})} \Delta a_{\ell,n^*} \right]} \\ &\leq C \Delta t_\ell^{1-\delta} \xrightarrow{\Delta t_\ell \rightarrow 0} 0. \end{aligned}$$

Finally, for I_3 , using Lemma 4.1 and Assumptions 4.2 and 4.3, we obtain

$$\begin{aligned} 0 \leq I_3 &\leq \frac{d_1^2 \Delta t_\ell^2 \mathbb{E}_{\pi_\ell} [|Y_\ell|^2]}{\mathbb{E}_{\pi_\ell} [Y_\ell^4]} = \frac{d_1^2 \Delta t_\ell^2 \mathbb{E}_{\pi_\ell} [\mathbb{E}_{\pi_\ell} [Y_\ell^2; (\mathcal{F}_{N_\ell}, \mathcal{I}_\ell^s = \mathcal{S})]]}{\mathbb{E}_{\pi_\ell} [\mathbb{E}_{\pi_\ell} [Y_\ell^4; (\mathcal{F}_{N_\ell}, \mathcal{I}_\ell^s = \mathcal{S})]]} \\ &= \frac{d_1^2 \Delta t_\ell^2 \mathbb{E}_{\pi_\ell} \left[\left((\Delta t_\ell^{\delta+1}) e^{2(\Delta t_\ell^{1-\delta} - \Delta t_\ell) \sum_{n \in \mathcal{S}} \Delta a_{\ell,n}} e^{-(\Delta t_\ell^{1-\delta} \Delta a_{\ell,n^*})} (\Delta a_{\ell,n^*}) (1 + h_{2,\ell}) \right) \right]}{\mathbb{E}_{\pi_\ell} \left[\left((\Delta t_\ell^{3\delta+1}) e^{4(\Delta t_\ell^{1-\delta} - \Delta t_\ell) \sum_{n \in \mathcal{S}} \Delta a_{\ell,n}} e^{-(\Delta t_\ell^{1-\delta} \Delta a_{\ell,n^*})} (\Delta a_{\ell,n^*}) (1 + h_{4,\ell}) \right) \right]} \\ &\leq \frac{d_1^2 \Delta t_\ell^{2(1-\delta)} \mathbb{E}_{\pi_\ell} \left[e^{2(\Delta t_\ell^{1-\delta} - \Delta t_\ell) \sum_{n \in \mathcal{S}} \Delta a_{\ell,n}} \Delta a_{\ell,n^*} (1 + h_{2,\ell}) \right]}{\mathbb{E}_{\pi_\ell} \left[e^{-(\Delta t_\ell^{1-\delta} \Delta a_{\ell,n^*})} \Delta a_{\ell,n^*} \right]} \\ &\leq \tilde{C} \Delta t_\ell^{2(1-\delta)} \xrightarrow{\Delta t_\ell \rightarrow 0} 0. \end{aligned}$$

Therefore, we conclude that

$$(A.5) \quad \mathbb{E}_{\bar{\pi}_\ell} \left[(Y_\ell - \mathbb{E}_{\bar{\pi}_\ell} [Y_\ell])^4 \right] \underset{\Delta t_\ell \rightarrow 0}{\sim} \mathbb{E}_{\bar{\pi}_\ell} [Y_\ell^4].$$

Finally, using (A.4), (A.5), Lemma 4.1 and Assumptions 4.2 and 4.3, we obtain

$$(A.6) \quad \begin{aligned} \kappa_\ell &:= \frac{\mathbb{E}_{\bar{\pi}_\ell} \left[(Y_\ell - \mathbb{E}_{\bar{\pi}_\ell} [Y_\ell])^4 \right]}{(\text{Var}_{\bar{\pi}_\ell} [Y_\ell])^2} \underset{\Delta t_\ell \rightarrow 0}{\sim} \frac{\mathbb{E}_{\bar{\pi}_\ell} [Y_\ell^4]}{(\mathbb{E}_{\bar{\pi}_\ell} [Y_\ell^2])^2} \\ &= \frac{\mathbb{E}_{\bar{\pi}_\ell} [\mathbb{E}_{\bar{\pi}_\ell} [Y_\ell^4(T); (\mathcal{F}_{N_\ell}, \mathcal{I}_\ell^s = \mathcal{S})]]}{(\mathbb{E}_{\bar{\pi}_\ell} [\mathbb{E}_{\bar{\pi}_\ell} [Y_\ell^2(T); (\mathcal{F}_{N_\ell}, \mathcal{I}_\ell^s = \mathcal{S})]])^2} \\ &= \Delta t_\ell^{\delta-1} \frac{\mathbb{E}_{\bar{\pi}_\ell} \left[e^{4(\Delta t_\ell^{1-\delta} - \Delta t_\ell) \sum_{n \in \mathcal{S}} \Delta a_{\ell,n}} e^{-(\Delta t_\ell^{1-\delta} \Delta a_{\ell,n^*})} \Delta a_{\ell,n^*} (1 + h_{4,\ell}) \right]}{\left(\mathbb{E}_{\bar{\pi}_\ell} \left[e^{2(\Delta t_\ell^{1-\delta} - \Delta t_\ell) \sum_{n \in \mathcal{S}} \Delta a_{\ell,n}} e^{-(\Delta t_\ell^{1-\delta} \Delta a_{\ell,n^*})} \Delta a_{\ell,n^*} (1 + h_{2,\ell}) \right] \right)^2} \\ &= \mathcal{O}(\Delta t_\ell^{\delta-1}). \end{aligned}$$

□

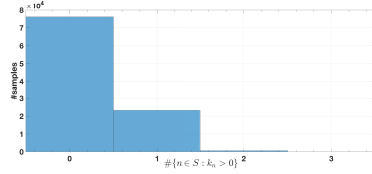
Proof of Theorem 4.2. Let $0 < \delta < 1$. Then, using (A.4), Lemma 4.1 and Assumptions 4.2 and 4.3, we obtain

$$(A.7) \quad \begin{aligned} \text{Var}_{\bar{\pi}_\ell} [Y_\ell] \underset{\Delta t_\ell \rightarrow 0}{\sim} \mathbb{E}_{\bar{\pi}_\ell} [Y_\ell^2] &= \mathbb{E}_{\bar{\pi}_\ell} [\mathbb{E}_{\bar{\pi}_\ell} [Y_\ell^2; (\mathcal{F}_{N_\ell-1}, \mathcal{I}_\ell^s = \mathcal{S})]] \\ &= \mathbb{E}_{\bar{\pi}_\ell} \left[\left(\Delta t_\ell^{\delta+1} \right) e^{2(\Delta t_\ell^{1-\delta} - \Delta t_\ell) \sum_{n \in \mathcal{S}} \Delta a_{\ell,n}} e^{-(\Delta t_\ell^{1-\delta} \Delta a_{\ell,n^*})} (\Delta a_{\ell,n^*}) (1 + h_{2,\ell}) \right] \\ &= \mathcal{O}(\Delta t_\ell^{1+\delta}). \end{aligned}$$

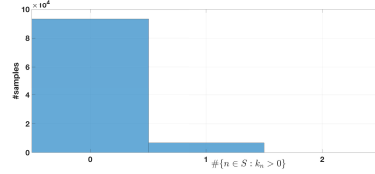
□

B Numerical Evidence of Assumption 4.1

In Figures B.1, B.2 and B.3, we plot the histograms, for Examples 5.1, 5.2 and 5.3, with $\delta = 0.5$, corresponding to $\#\{\text{IS steps : s.t. } \bar{K} := \sum_{j \in \mathcal{J}_1} \sum_{n \in \mathcal{S}_j} k_n^j > 0\}$, that is the number of times where we perform IS and succeeded to separate the two paths. These Figures show that our assumption 4.1 (c) is valid since for small values of Δt_ℓ , we have at most one jump created by IS such that it separates the two paths.

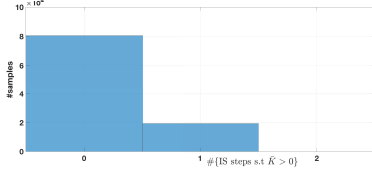


(a)

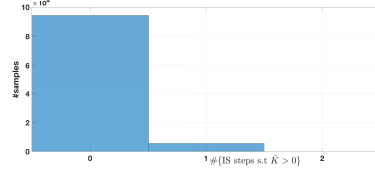


(b)

Figure B.1: Example 5.1 with IS (with $\delta = 0.5$): Histogram of $\#\{n \in \mathcal{S} : k_n > 0\}$, for number of samples $M_\ell = 10^5$. a) $\ell = 6$. b) $\ell = 10$

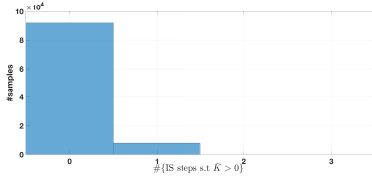


(a)

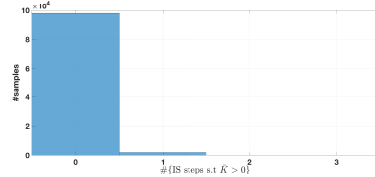


(b)

Figure B.2: Example 5.2 with IS (with $\delta = 0.5$): Histogram of $\#\{\text{IS steps : s.t. } \overline{K} := \sum_{j \in \mathcal{J}_1} \sum_{n \in \mathcal{S}_j} k_n^j > 0\}$, for number of samples $M_\ell = 10^5$. a) $\ell = 4$. b) $\ell = 8$.



(a)



(b)

Figure B.3: Example 5.3 with IS (with $\delta = 0.5$): Histogram of $\#\{\text{IS steps : s.t. } \overline{K} := \sum_{j \in \mathcal{J}_1} \sum_{n \in \mathcal{S}_j} k_n^j > 0\}$, for number of samples $M_\ell = 10^5$. a) $\ell = 6$. b) $\ell = 10$